




Identification of the ejecta deposit formed by the Australasian Tektite Event at Huai Om, northeastern Thailand

Toshihiro TADA ^{1*}, Ryuji TADA^{1,2,3}, Paul A. CARLING⁴, Wickanet SONGTHAM⁵, Praphas CHANSOM⁵, Toshihiro KOGURE², Yu CHANG ^{2,6}, and Eiichi TAJIKA ²

¹Institute for Geo-Cosmology, Chiba Institute of Technology, 2-17-1 Tsudanuma, Narashino, Chiba 275-0016, Japan

²Department of Earth and Planetary Science, The University of Tokyo, 7-3-1 Hongo, Bunkyo-Ku, Tokyo 113-0033, Japan

³Research Center for Earth System Science, Yunnan University, Chenggong District, Kunming 650500, People's Republic of China

⁴Geography and Environmental Sciences, University of Southampton, Highfield, Southampton SO17 1BJ, UK

⁵Northeastern Research Institute of Petrified Wood & Mineral Resources, Nakhon Ratchasima Rajabhat University, Baan Kroke Duen Ha, Suranaree Sub-district, Muang Nakhon Ratchasima District, Nakhon Ratchasima 30000, Thailand

⁶Present address: Google, Shibuya-City, Tokyo, Japan G.K.

*Corresponding author. E-mail: tada.toshihiro@p.chibakoudai.jp

(Received 08 April 2022; revision accepted 25 July 2022)

Abstract—The Australasian Tektite Event, approximately 0.8 Ma, is the youngest record of a large impact event on Earth. Although it is estimated that it occurred somewhere in Indochina based on the distribution of tektites, the crater has never been located. Here, we report the discovery and occurrence of shocked quartz with planar deformation features (PDFs) in the Quaternary depositional sequence at Huai Om in northeastern Thailand. Measurements of the orientation of lamellae using a universal stage microscope as well as observation using scanning electron microscopy and transmission electron microscopy were conducted to confirm the presence of PDFs. Together with the occurrence of in situ layered tektite fragments, we identify the depositional sequence as the ejecta deposit formed by the Australasian Tektite Event. We further describe the detailed lithostratigraphy of the ejecta deposit, which will allow the tracing of its distribution and lateral changes in its thickness, grain size, and grain composition. Further investigation of the lateral distribution of the ejecta deposit would provide information about the location, magnitude, and target rocks of the Australasian Tektite Event.

INTRODUCTION

Background

Impacts of large extraterrestrial bodies can cause catastrophic effects on the environment of the Earth. Although ~200 impact craters have been identified on Earth (Schmieder & Kring, 2020), previous studies on environmental effects of large impacts have been conducted mostly on the K/Pg event (Alvarez et al., 1980; Pierazzo & Artemieva, 2012; Schulte et al., 2010). In general, the study of impact events on Earth is difficult because the geological evidence of impacts, such as craters and proximal ejecta layers, has been erased over time due to weathering, erosion, burial, and

tectonics. Thus, evidence of impacts and their environmental perturbations more likely is preserved for younger impacts. It is, therefore, important to study young impact events.

In this context, the Australasian Tektite Event (AATE), which occurred at approximately 0.8 Ma (788.1 ± 3.0 ka [Jourdan et al., 2019]; 793 ± 14 ka [Schwarz et al., 2016]; 800 ± 6 ka [Yamei et al., 2000]), is important because it is the youngest known large impact event on Earth. The Australasian tektite strewn field, extending across Indochina through Australia to Antarctica (Fig. 1a) (e.g., Folco et al. [2016] and references therein), is the largest and youngest known tektite strewn field. The size of the source crater has been estimated to be between 30 and 120 km in diameter based

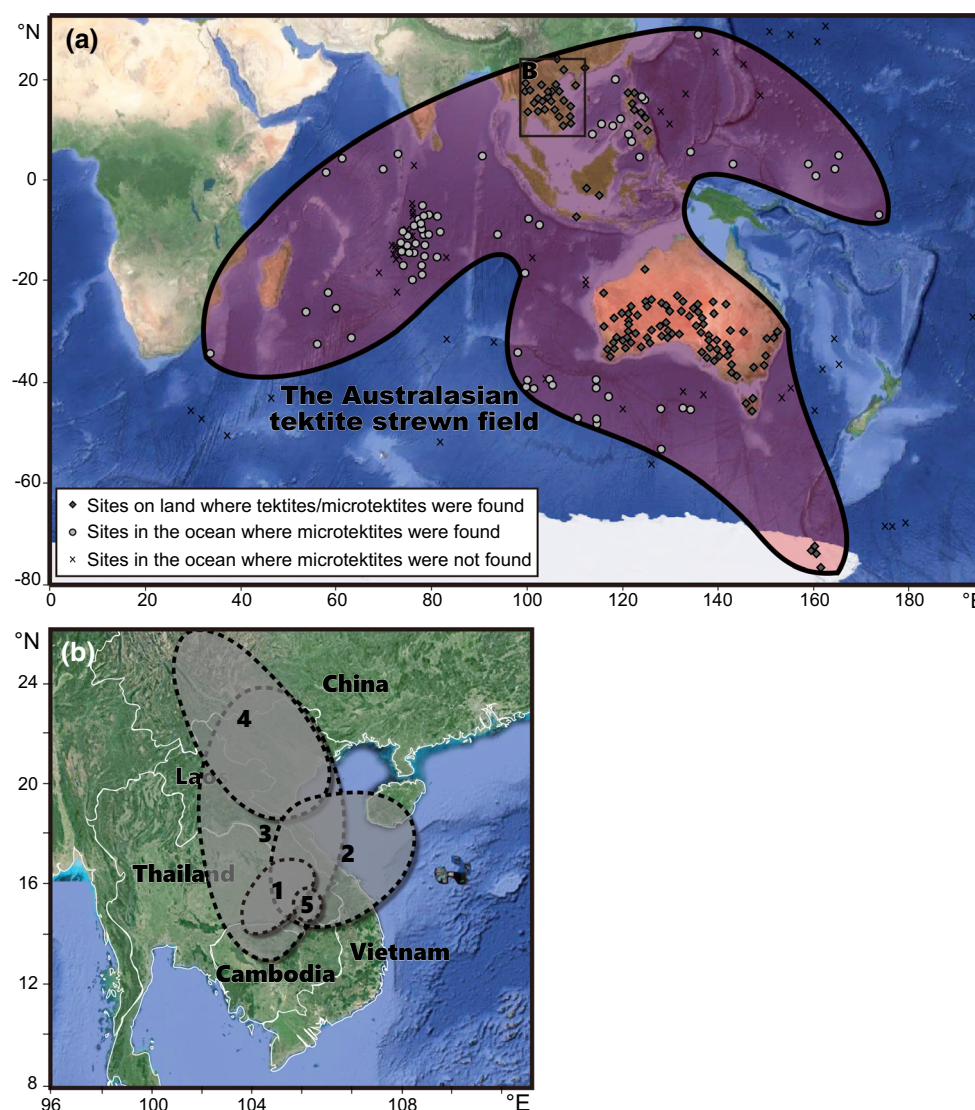


Fig. 1. a) Distribution of the Australasian tektites. The solid line indicates the boundary of the strewn field defined by the occurrence of the microtektites in marine sediment cores and on Antarctica (after Folco et al., 2011). The sites where tektites are found on land are after Folco et al. (2011) and Glass and Koeberl (2006). b) Estimated areas for the location of the AATE. (1) Schnetzler (1992), (2) Ma et al. (2004), (3) Glass and Koeberl (2006), (4) Prasad et al. (2007), (5) Sieh et al. (2020). (Color figure can be viewed at [wileyonlinelibrary.com](https://onlinelibrary.wiley.com/terms-and-conditions).)

on the thickness distribution of the microtektite layer in marine sediment cores (Glass & Koeberl, 2006; Glass & Pizzuto, 1994; Lee & Wei, 2000; Prasad et al., 2007). Despite the large magnitude and young age of the impact, the source crater of the AATE has not been conclusively identified to date. Thus, the nature of the impact, such as the location, magnitude, impact angle and direction, and types of the target rock, is not well understood.

Previous researchers estimate the location of the impact to be somewhere in the eastern part of Indochina based on the distribution of the tektites on land and microtektites in marine sediment cores (Glass & Koeberl,

2006; Ma et al., 2004; Prasad et al., 2007; Schnetzler, 1992; Sieh et al., 2020) (Fig. 1b). In particular, the limited distribution of the layered (Muong Nong-type; MN) tektites, which are considered to be proximal to the impact site (e.g., Koeberl, 1992), suggests that the crater is in the area around northeastern Thailand and southwestern Laos (Schnetzler, 1992). Recently, Sieh et al. (2020) proposed that the impact took place on the basalt field of the Bolaven Plateau in southwestern Laos and the crater was buried by younger basalt erupted after the impact, based on the presence of a basalt component in the geochemistry of the tektites, pre-impact and postimpact ages of the basalt, negative gravity anomaly

in the basalt field, and the presence of a possible ejecta deposit in southern Laos.

Because the thickness of an ejecta layer varies in accordance with the distance from the crater and the magnitude of the impact (e.g., McGetchin et al., 1973), the thickness distribution of the ejecta layer could provide useful information to specify the location and magnitude of the impact. Although the distal ejecta layer of the AATE has been recognized as the microtektite layer in marine sediment cores at multiple locations (e.g., Prasad et al., 2007), the ejecta layer of the AATE has never been conclusively identified on land in Indochina.

There are several sites in Indochina where tektites have been reported from the Quaternary depositional sequence (Barnes & Pitakpaivan, 1962; Fiske et al., 1996, 1999; Schnetzler & McHone, 1996; Songtham et al., 2011, 2012; Tada et al., 2020; Tamura, 1992; Wasson et al., 1995). In these cases, tektites are found from the upper part of or at the top of a so-called “laterite” layer, which is a loose nodular reddish-black ferruginous layer broadly distributed a few meters below the surface in Southeast Asia. Several authors considered that the tektites in the “laterite” layer were directly deposited in the strata (Nuchanong et al., 2014; Songtham et al., 2011, 2012; Tamura, 1992; Wongsomsak, 1986), and there is a possibility that the tektite-bearing “laterite” layer is a part of the ejecta deposit of AATE (Tada et al., 2020). The possibility of reworking of tektites after the impact has been claimed due to the lack of detailed sedimentological description of tektites and tektite-bearing deposits and the lack of other evidence of impact, such as shock deformation features in minerals (Fiske et al., 1996; Keates, 2000; Koeberl & Glass, 2000; Langbroek, 2015).

Sieh et al. (2020) reported that the bouldery breccia in southern Laos may be a possible ejecta deposit, based on the findings of quartz grains with apparent planar microstructures that they believe to be planar deformation features (PDFs), a diagnostic feature to identify shocked quartz. However, Sieh et al. (2020) did not conduct comprehensive identification of PDFs, which is usually required for identification of shocked quartz, as discussed in detail in the next section. In addition, lithostratigraphic and petrographic occurrence of the possible shocked quartz grains and the bouldery breccia was not described.

Recently, Tada et al. (2020) reported on the detailed occurrence of tektite fragments in the upper part of the “laterite” layer at HO06 section near Huai Om, northeastern Thailand. They demonstrated that the tektite fragments were formed by fragmentation of one large tektite mass at the time of the landing after the ejection by the impact, and have not been disturbed

further (i.e., the tektite fragments are in situ) based on the angular shapes, size distribution, similar chemical composition of the tektite fragments, and the fact that the fragments can be fitted together to form one large (~370 g) ellipsoidal MN tektite mass. However, evidence of the impact metamorphism other than the tektite fragments (such as shock deformation features in minerals) was not described from the strata.

In this study, we report the detailed lithostratigraphy of the Quaternary sequence, including the “laterite” layer and discovery of shocked quartz with PDFs from the sequence at Huai Om, northeastern Thailand. Based on these findings, in addition to the occurrence of recently discovered MN tektite fragments near Huai Om (Tada et al., 2020), we propose that the Quaternary depositional sequence at Huai Om is the ejecta deposit of the AATE.

We further conduct a lithostratigraphic subdivision of the ejecta deposit and discuss their possible depositional processes. The result of this study will provide lithostratigraphic criteria to identify the proximal ejecta deposit of this impact event that will be useful to trace their lateral distribution with respect to the thickness, grain size, and composition.

Criteria to Identify PDFs in Quartz

Quartz is the most commonly used mineral indicator of shock metamorphism because of its abundance, resistance to chemical and physical alteration, and tendency to develop striking and unique deformation features (e.g., French & Koeberl, 2010; Stöffler & Langenhorst, 1994). In particular, PDFs in quartz have been used as the most robust indicator of shock metamorphism. PDFs are single or multiple sets of parallel and planar lamellae oriented in specific crystallographic planes and generated at shock pressures >~8 GPa (e.g., Chao, 1967; French & Koeberl, 2010; Stöffler & Langenhorst, 1994).

However, under an optical microscope, deformation lamellae in quartz formed by tectonic deformation can, in some cases, resemble PDFs. There are several examples where tectonic deformation lamellae were misinterpreted as PDFs or still remain controversial due to insufficient observations (e.g., Cordier et al., 1994; Glikson, 2004; Langenhorst & Deutsch, 1996; Langenhorst et al., 2005; Leroux & Doukhan, 1993; Reimold et al., 2014). Thus, discrimination of PDFs from tectonic deformation lamellae requires careful investigation and experience (see discussion in, e.g., French & Koeberl, 2010; Gratz et al., 1996; Hamers & Drury, 2011; Reimold et al., 2014; Stöffler & Langenhorst, 1994).

In this section, we briefly review the characteristic differences between PDFs and tectonic deformation lamellae in quartz, which have been used as the criteria

for discriminating PDFs and tectonic deformation lamellae. The criteria can be listed as (1) spacing of lamellae; (2) thickness of lamellae; (3) crystallographic orientations of lamellae; (4) number of sets of lamellae per grain; (5) component of lamellae; and (6) sharpness, parallelism, and linearity of lamellae (e.g., French & Koeberl, 2010; Grieve et al., 1996; Reimold et al., 2014; Stöffler & Langenhorst, 1994).

1. *Spacing of lamellae*: Spacing of PDFs in quartz ranges from about 2 to 10 μm under an optical microscope and <1 to $\sim 4 \mu\text{m}$ under TEM (transmission electron microscope; e.g., Goltrant et al., 1992; Langenhorst, 1994). The spacing of the tectonic deformation lamellae is generally $>5 \mu\text{m}$ and tends to be wider than the spacing of PDFs (e.g., Alexopoulos et al., 1988; Vernooij & Langenhorst, 2005).
2. *Thickness of lamellae*: The thickness of PDFs in quartz is typically $<1 \mu\text{m}$ (e.g., Ashworth & Schneider, 1985; Goltrant et al., 1992) and $2 \mu\text{m}$ as a maximum (Hough et al., 2003; Stöffler & Langenhorst, 1994). The thickness of tectonic deformation lamellae is $>2 \mu\text{m}$ and thicker than PDFs (e.g., Drury, 1993; McLaren & Hobbs, 1972).
3. *Orientation of lamellae*: PDFs are oriented parallel to specific crystallographic planes most commonly with low Miller–Bravais indices, such as $\omega\{10\bar{1}3\}$, $\pi\{10\bar{1}2\}$, and $c(0001)$ (e.g., Ferrière et al., 2009; French & Koeberl, 2010; Stöffler & Langenhorst, 1994). The orientations of tectonic deformation lamellae are not crystallographically controlled. As a result, frequency distribution plots of polar angles of tectonic deformation lamellae form a bell-shaped curve with a broad maximum, while plots of PDF poles are concentrated into sharp peaks at the polar angles associated with specific lattice planes (e.g., Ferrière et al., 2009; French & Koeberl, 2010; Stöffler & Langenhorst, 1994).
4. *Number of sets of lamellae per grain*: PDFs present single or multiple sets (1–18 sets) per grain, while tectonic deformation lamellae mostly present a single set and rarely present two sets (extremely rarely more sets) per grain (e.g., French & Koeberl, 2010; Hamers & Drury, 2011; Lyons et al., 1993; Stöffler & Langenhorst, 1994).
5. *Component of lamellae*: Based on TEM observations, PDFs largely are classified into two types: nondecorated type and decorated type (French & Koeberl, 2010; Goltrant et al., 1991; Gratz et al., 1992; Grieve et al., 1996; Stöffler & Langenhorst, 1994). Nondecorated type PDFs are composed of amorphous SiO_2 glass, or a mixture of amorphous silica and tiny crystalline quartz (e.g., Goltrant et al., 1992). Decorated type PDFs are

composed of narrow bands of tiny ($\sim 0.1 \mu\text{m}$ sized) vugs or narrow bands of dislocations decorated with tiny vugs (e.g., Goltrant et al., 1991, 1992). In most cases, tectonic deformation lamellae occur as elongated subgrains associated with subgrain boundaries, across which the orientation of the crystal changes slightly (Cordier et al., 1994; Drury, 1993; Joreau et al., 1996; Langenhorst & Deutsch, 1996; McLaren & Hobbs, 1972; Vernooij & Langenhorst, 2005; White, 1973).

6. *Sharpness, parallelism, and linearity of lamellae*: Generally, PDFs are sharp, plane-parallel, and linear (French & Koeberl, 2010; Stöffler & Langenhorst, 1994; von Engelhardt and Bertsch 1969). In most cases, tectonic deformation lamellae in quartz are clearly curved or sinuous, less parallel, and more vague than PDFs (e.g., French & Koeberl, 2010; Reimold et al., 2014). However, in some cases, tectonic deformation lamellae can be subparallel to parallel and sublinear to linear, resulting in an apparent resemblance to PDFs under an optical microscope (French & Koeberl, 2010). In addition, if a shocked quartz grain is strained before or after impact deformation, PDFs may give the appearance of being slightly curved because they follow the lattice orientation strained through the grain (Reimold et al., 2014). It is also known that if PDFs are obliquely oriented with shallow angles to the thin section plane, they appear as broad, vague, and subplanar features (Reimold et al., 2014). In these cases, it is more difficult to discriminate PDFs from tectonic deformation lamellae by observation under an optical microscope.

Consequently, in most cases, PDFs and tectonic deformation lamellae can be discriminated by careful observation under an optical microscope in respect of their thickness, spacing, number of sets per grain, sharpness, parallelism, and linearity (e.g., French & Koeberl, 2010; Stöffler & Langenhorst, 1994). However, in some cases, the microscopic appearance of PDFs and tectonic deformation lamellae can show some similarities. Thus, in such cases, the observation of lamellae under an optical microscope is insufficient, and the measurement of orientations of lamellae and/or SEM (scanning electron microscopy)/TEM observations of lamellae are mandatory for definitive identification of PDFs (French & Koeberl, 2010; Stöffler & Langenhorst, 1994).

Previous Study Searching for Shocked Quartz on Land in Indochina

Although shocked quartz grains from the Australasian microtektite layer are found in marine sediment cores (Campanale et al., 2019; Folco et al.,

2010; Glass & Koeberl, 2006; Glass & Wu, 1993), shocked quartz grains have not been identified conclusively from the Quaternary deposits on land in Indochina.

Howard et al. (2000) reported quartz grains with possible PDFs in the large flood deposits immediately above the tektite-bearing “laterite” layer at Ban Tha Chang sandpit in northeastern Thailand, but measurement of the orientation of the lamellae and/or SEM/TEM observation were not conducted.

Sieh et al. (2020) proposed that the bouldery breccia in southern Laos is a possible ejecta deposit based on the findings of quartz grains with apparent planar microstructures that they believe to be PDFs. However, they did not conduct comprehensive measurements of the orientation of the lamellae to identify PDFs. In order to identify PDFs, more than 50–100 measurements of the lamellae are necessary (Ferrière et al., 2009), while Sieh et al. (2020) measured only 14 angles between the quartz *c*-axis and poles to the lamellae, which cluster around 52° and 66°. These angles are, however, not the common orientations of PDFs (e.g., French & Koeberl, 2010). In addition, the spacing of the lamellae in the quartz grains reported in Sieh et al. (2020) is slightly wider (2–18 µm) than that of PDFs in shocked quartz (2–10 µm; e.g., Ferrière et al., 2009; Stöffler & Langenhorst, 1994). SEM/TEM observations of the lamellae were not conducted by Sieh et al. (2020). Consequently, their identification of shocked quartz is not convincing. Thus, shocked quartz has never been identified convincingly in the Quaternary deposits, and the ejecta layer formed by this impact event has never been identified on land in Indochina.

STUDY SITE AND GEOLOGICAL SETTING

We conducted a field survey at Huai Om section located near the southeastern margin of the Khorat Plateau in northeastern Thailand, about 80 km southeast from Ubon Ratchathani (Fig. 2). The Huai Om section is exposed downstream of the Huai Om dam spillway, where the Cretaceous sedimentary basement and overlying Quaternary deposit, which dips 4° to the west, are continuously exposed laterally for at least 300 m. Two subsections A and B were examined along the exposure. The Huai Om section was previously studied by Fiske et al. (1996), who reported MN tektites from the top of the “laterite” layer.

The Khorat Plateau Basin is filled with Mesozoic sedimentary rocks (Khorat Group; Minezaki et al., 2019; Racey et al., 1996). The Khorat Group is composed mainly of nonmarine sandstone and mudstone with minor presence of conglomeratic sandstone (Racey et al., 1996). The Quaternary deposits

unconformably overlie the Mesozoic sedimentary basement. The typical thickness of the Quaternary deposits in the Khorat Plateau Basin, along the main rivers (Mun and Chi rivers), is 35–80 m (Nuchanong et al., 2014). The Quaternary deposits are composed of gravel beds that are considered as river terrace deposits (Nuchanong et al., 2014; Tamura, 1992) at the base, which is overlain by the “laterite” layer and then by the fine to medium sand layer in ascending order (e.g., Songtham et al., 2011, 2012). Away from the main rivers, the Quaternary deposits are devoid of river terrace deposits and the “laterite” layer lies directly on the Mesozoic basement. The thickness of the “laterite” layer plus the overlying fine to medium sand layer is several meters (Fiske et al., 1996; Tamura, 1992).

METHODS

Field Observation and Sampling

Field survey was conducted at the Huai Om section to describe the occurrence of shocked quartz grains and the lithostratigraphy of the shocked quartz-bearing Quaternary deposit. Because a large part of the outcrop was covered by vegetation, we cleaned the outcrop to make complete exposure from the basement sandstone to the top of the Quaternary deposit at the two subsections A and B (Fig. 2c). Then, we further cleaned the exposed surface with scrapers and brushes to make columnar sections with millimeter resolution.

Twenty sediment samples were taken at 10–50 cm intervals at subsection A (Fig. 3). These samples were subjected to grain size analysis (12 samples), and thin section observations (20 samples) to investigate lithostratigraphy and if shocked quartz grains were present or not (Fig. S1 in supporting information). A slab section (25 cm wide, 10 cm high, and 5 cm thick) was taken from the “laterite” layer at subsection A, which was resin-indurated and polished to observe shape and composition of gravel clasts. Seven thin sections were made from the slab section (thin sections HUnit2-1–7).

Roundness Analysis of Gravels in the “Laterite” Layer

The outlines of gravel particles with axes longer than 0.4 cm were traced on photographs of the polished surface of the “laterite” sample (Fig. S2 in supporting information). Roundness (*R*), defined by Takashimizu and Iiyoshi (2016), was measured using the image processing software ImageJ (Abramoff et al., 2004; Schneider et al., 2012). *R*-values were converted to the traditional roundness index (*R_k*) of Krumbein (1941) according to Takashimizu and Iiyoshi (2016).

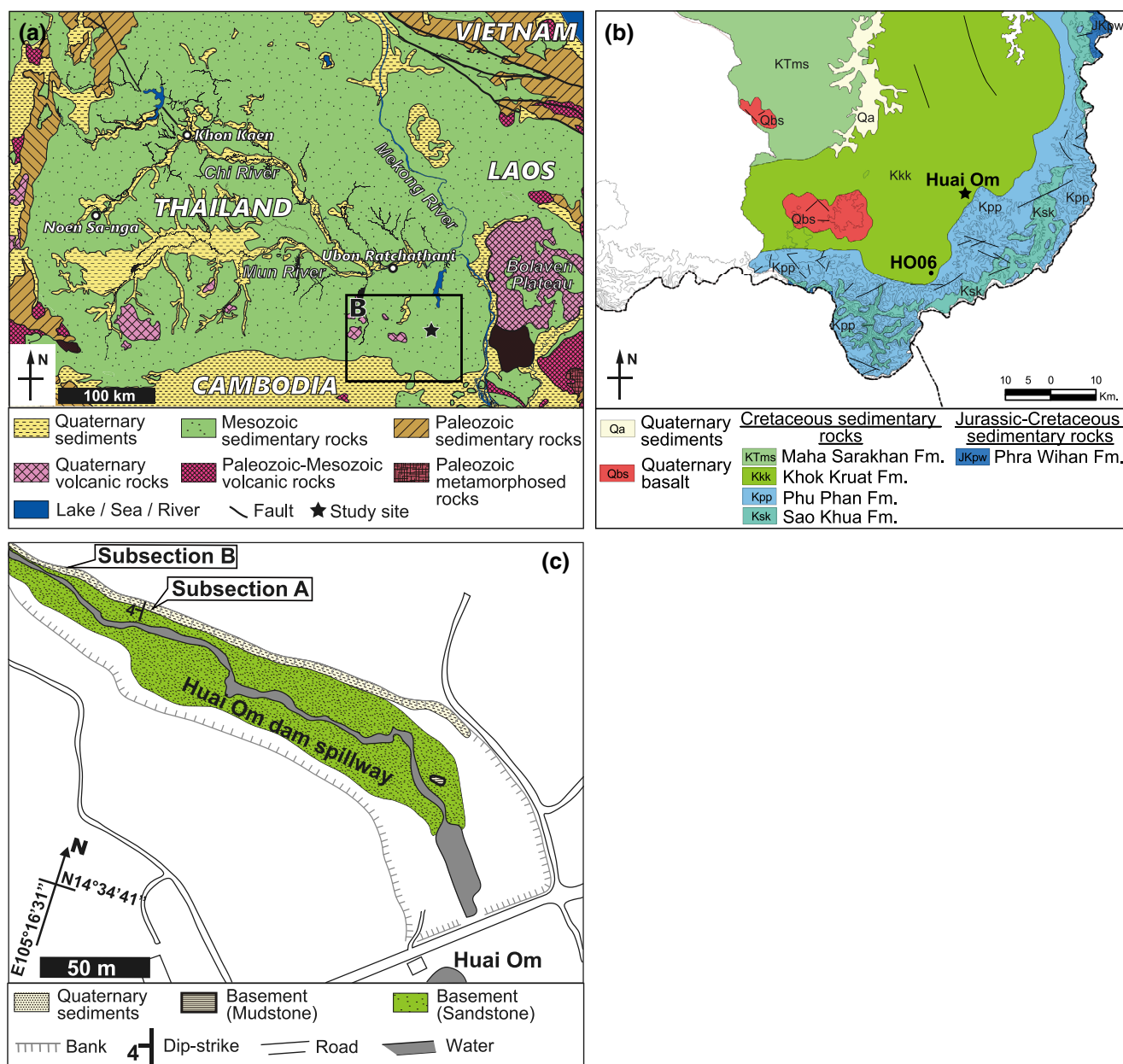


Fig. 2. a) Geological map of the Khorat Plateau Basin (modified from Teraoka & Okumura, 2011). The location of the study site is also shown. b) Geological map of the southern part of Ubon Ratchathani province, northeastern Thailand (after the geological map of Thailand by province made by Department of Mineral Resources of Thailand; http://www.dmr.go.th/n_more_news.php?nid=79591, accessed December 15, 2020). c) Route map of the Huai Om section. (Color figure can be viewed at wileyonlinelibrary.com.)

Grain Size Analysis

Twelve samples were disaggregated in deionized water and sieved through a 2 mm mesh. The <2 mm fraction of each sample was subject to grain size analysis using a Malvern Mastersizer 2000 laser diffraction grain size analyzer (Appendix S2 in supporting information). Before these analyses, organic matter, carbonate, and

iron and manganese oxide cements were removed by chemical pretreatments (Appendix S2).

Measurement of Orientations of Lamellae in Quartz

The orientations of lamellae were measured on 36 thin sections through the Quaternary sequence (Fig. S1) under a polarized microscope with a four-axis universal

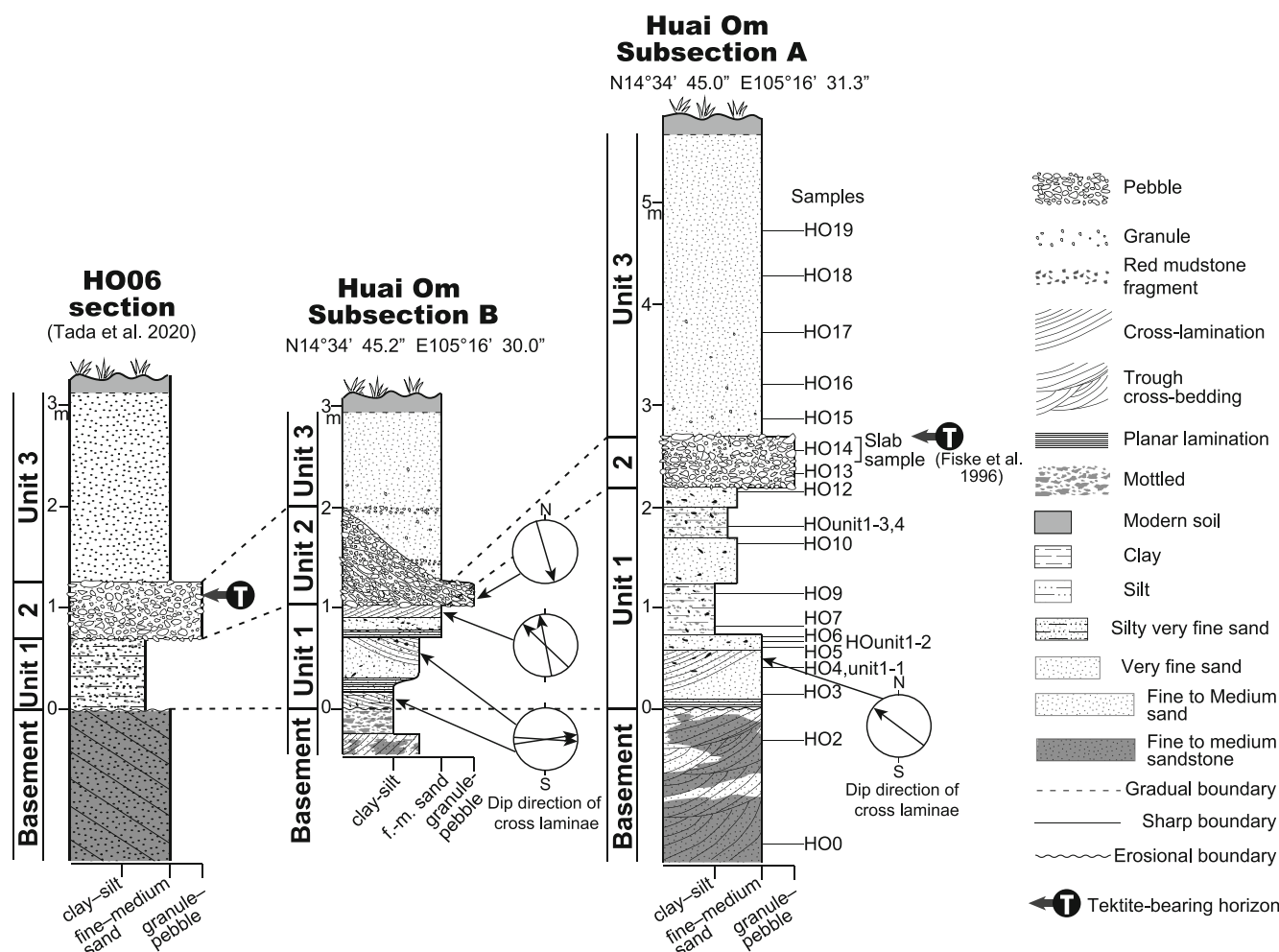


Fig. 3. Columnar sections at Huai Om subsections A and B showing basement sedimentary rocks and the overlying three lithostratigraphic Units 1–3 correlated with the columnar section at nearby HO06 section (Tada et al., 2020). Dip directions of the cross-stratification are also shown.

stage at the University of Tokyo, based on the method of Stöffler and Langenhorst (1994), Langenhorst (2002), and Ferrière et al. (2009). The orientations of lamellae were indexed to the orientations of PDFs by the manual indexing method (e.g., Stöffler & Langenhorst, 1994) using the stereographic projection template proposed by Ferrière et al. (2009) and assuming a 5° measurement error (e.g., Stöffler & Langenhorst, 1994). First, the orientations (azimuth and inclination angles) of the quartz *c*-axis and the normal to the lamellae plane were measured using the universal stage microscope, and angles between the *c*-axis and poles of the lamellae were calculated. Then, the measured orientations were plotted in a stereographic Wulff net (equal angle projection) and compared with the standard stereographic projection of PDFs in shocked quartz (Ferrière et al., 2009). The azimuth and inclination angles were measured twice, rotating the stage 180°. The stereonet projection, angle, and rotation calculations were conducted using Stereonet

11 software (Allmendinger et al., 2011; Cardozo & Allmendinger, 2013). The crystallographic orientations of 154 lamellae sets in 125 grains in total were measured.

SEM/TEM Observations of Lamellae in Quartz

One quartz grain with the lamellae (grain no. 211205-1) on the polished thin section HO10-1 was investigated using SEM at the Planetary Exploration Research Center, Chiba Institute of Technology, using JEOL JSM-6500LA operated at 15 kV. The thin section was coated with a thin carbon film on the surface using vacuum evaporation before the SEM observation.

In addition, one quartz grain with the lamellae (grain no. 19d-3) on the polished thin section HO19 was investigated using SEM/TEM at the University of Tokyo. A 5 mm-sized piece of the polished thin section, containing the quartz grain, was chemically etched with hydrofluoric vapor after the method of Christie

et al. (1964) and Gratz et al. (1996). After the etching, a thin carbon film was coated on the surface by vacuum evaporation for SEM observation. SEM observation was conducted using a Hitachi S-4500 SEM with a cold-type field-emission electron gun operated at 5 kV. An ultrathin section for TEM observation was prepared from the etched surface as the section was perpendicular to lamellae identified by SEM, using a focused ion beam (FIB) system with a microsampling function (Hitachi FB-2100). The ultrathin section was examined by TEM, using a JEOL JEM-2010 operated at 200 kV.

Analysis of the Abundance of Quartz Grains with PDFs

Analysis of the abundance of shocked quartz grains (percentage of the quartz grains with PDFs among all quartz grains observed) was conducted for three thin sections (HUnit1-1, HUnit2-1, HO19). The thin sections were observed under the universal stage microscope. Shocked quartz grains with PDFs and quartz grains without PDFs were counted and the abundance of shocked quartz grains was calculated.

RESULTS

Lithostratigraphy of the Quaternary Sequence at Huai Om Section

Field Observation

Basement: The basement rock at the Huai Om section is composed of purple-gray sandstone and red mudstone of the Cretaceous Khok Kruat Formation in the uppermost part of the Khorat Group (Nuchanong et al., 2014). The basement sandstone is exposed continuously along the spillway of Huai Om section. The sandstone, which dips 4° to the west, shows trough cross-bedding with a current direction being consistently to N65°–80°W throughout the outcrop. The uppermost 1.2 m of the basement sandstone is partly altered to be softer and fragile showing whitish-gray color at subsection A (Fig. 4). Because the boundary between the whitish-gray altered part and the purple-gray (less altered) part is gradual and the cross-bedding structure continues across the color boundary, the color alteration is a secondary feature, probably due to weathering (Fig. S3 in supporting information). A massive red mudstone, which is intercalated in the purple-gray sandstone, is observed at subsection B and locally along the spillway (Figs. 3 and 5; Fig. S4 in supporting information). The exposed thickness of this mudstone is about 10 cm, but the total thickness could be greater. The Quaternary sediments overlying the Cretaceous basement can be divided into three lithostratigraphic units (Units 1–3 in ascending order; Figs. 3–5).

Unit 1: Unit 1 is composed of decimeter-scale alterations of whitish gray silt and fine sand layers that contain various amounts of red mudstone clasts. The amount of the red mudstone clasts is larger in the silt layers than in the sand layers. The thickness of this unit is 2.2 m at subsection A and 1.0 m at subsection B. The basal contact of this unit is sharp and relatively planar and forms a low angle angular unconformity. The dip and strike of the basal contact is N72°W2°N at subsection A and N30°W6°E at subsection B suggesting that the basal contact is slightly undulating. The presence of the red mudstone clasts, which are considered to be rip-up clasts of the basement red mudstone, indicates that the basal contact is erosional (Fig. 5e; Fig. S5 in supporting information). The whitish-gray sand layer in the lower part of subsection A shows cross-stratification, which dips to N51°W. The cross-stratification in Unit 1 at subsection B dips to N81°E and N94°E in the lower part and N12°–46°W at the uppermost part (Fig. 3).

Unit 2: Unit 2 is a reddish-brown sandy granule to pebble layer. The boundary between Units 1 and 2 is sharp and generally planar, and there is no evidence of erosion (Figs. 4 and 5). The thickness of this unit is 50 cm at subsection A, while it varies from 20 cm to 1 m with a wavy upper boundary at 1.2 m wide subsection B (Fig. 5). This layer is poorly sorted, and the gravel clasts are partly grain-supported (Fig. 6a). This unit is generally structureless, but the lower part of this unit at subsection B shows cross-bedding dipping to N164°E (Fig. 3). The gravel clasts are 0.2–3 cm in diameter, rounded to angular, and composed mainly of white quartzite pebbles, with a minor amount of red and green mudstone, and red and gray sandstone fragments. This unit is partly cemented by reddish-brown iron oxides in a manner similar to the so-called “laterite” layer (Songtham et al., 2011, 2012) (Fig. 6a).

Unit 3: Unit 3 is composed of a whitish to light brownish gray massive fine to medium sand. The thickness of this unit is 3 m. It overlies Unit 2 with a sharp and planar contact at subsection A, and a sharp and wavy contact at subsection B with no evidence of erosion (Figs. 4 and 5). Unit 3 is capped by approximately 20 cm of modern soil with a gradational contact. The fine to medium sand of this unit is well sorted compared to Unit 2 (Figs. S6 and S7 in supporting information). The lower 1.5 m of the layer sparsely contains angular white quartzite granules. Thin granule to pebble layers, which are not continuous laterally, are observed in the bottom of this unit at subsection B.

Thin Section and Slab Section Observation

The basement sandstone is a quartz arenite mostly composed of quartz with minor plagioclase, mudstone fragments and opaque minerals, and a trace amount of

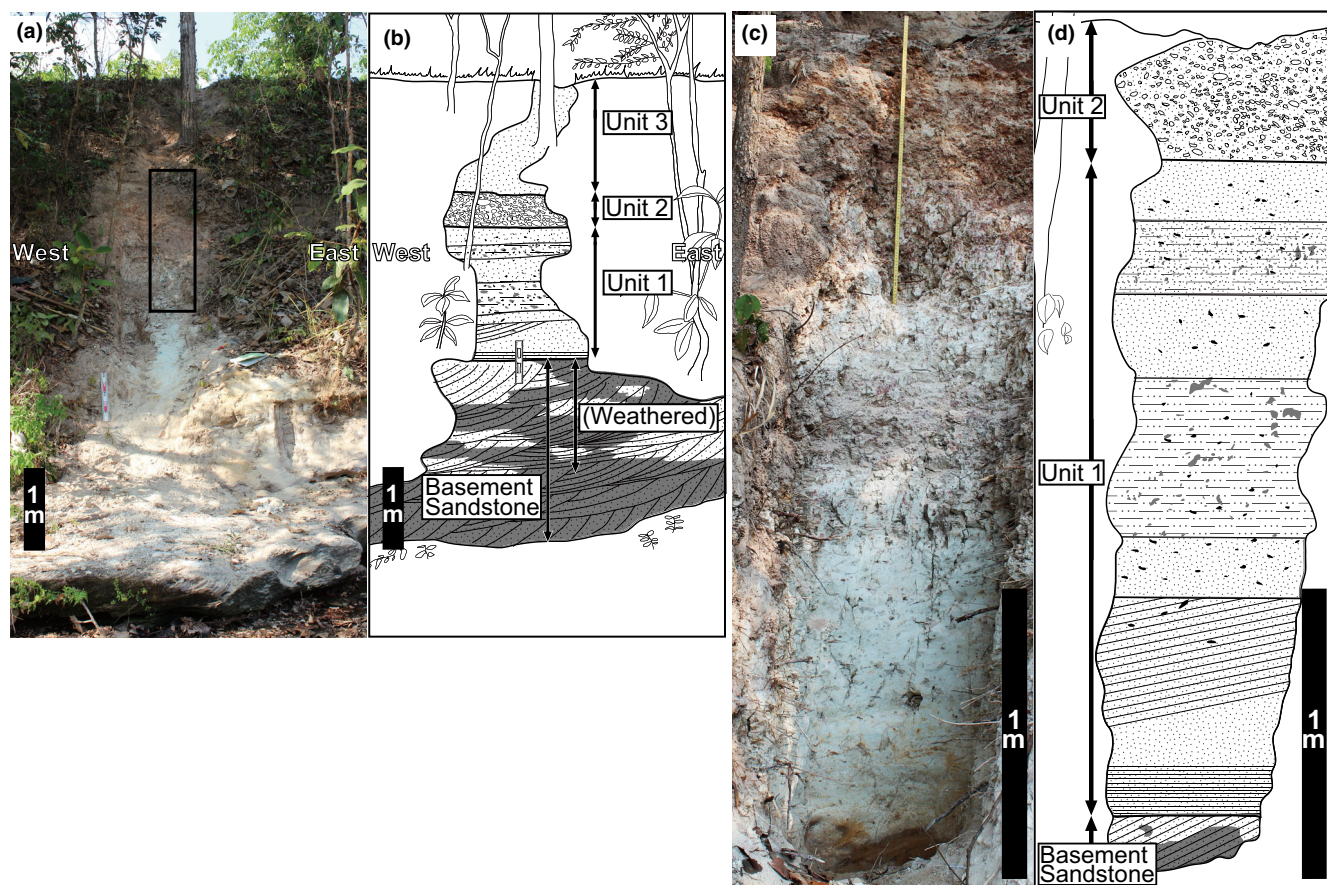


Fig. 4. a and b) A field photograph and its sketch of subsection A at Huai Om showing the division of Units 1–3. c and d) An enlarged photograph and its sketch of Units 1 and 2. The position of the photograph (c) is indicated with the rectangle in (a). Legends for the sketches are same as Fig. 3. (Color figure can be viewed at wileyonlinelibrary.com.)

muscovite, olivine, and zircon. The sand grains are mainly 100–300 μm in size, and a clay-size matrix is minor (Figs. S3a and S6). The weathered whitish-gray part of the basement sandstone is mostly composed of quartz with minor amount of plagioclase, mudstone fragments, and rare olivine and zircon. The size of sand grains is similar to the unaltered part, but the amount of clay-size matrix is much larger (Figs. S3c and S6).

The whitish-gray sand layers in Unit 1 are mostly composed of single-crystal quartz and mudstone fragments with a minor amount of biotite and muscovite and rare zircon, which are similar in composition to the weathered part of the basement (Fig. S8a in supporting information). The size of sand grains and the abundance of clay-size matrix are also similar to the weathered basement (Fig. S6). The whitish-gray silt and silty very-fine sand layers in Unit 1 are mostly composed of single-crystal quartz, mudstone fragments, and opaque minerals with a minor amount of zircon, biotite, and muscovite with clay-size matrix. The amount of clay-size matrix is much larger than that of the sand layers in Unit 1

(Figs. S5 and S6). Medium- to coarse (200–300 μm)-sized quartz grains are present but rare.

The gravel clasts in Unit 2 are composed mainly of metaquartzite. Red and gray medium-grained sandstone fragments and green and red mudstone fragments also are observed in a small amount (approximately 10%; Fig. S9 in supporting information). These gravel clasts in Unit 2 are considered to be derived from the basement sedimentary rocks (sandstone, mudstone, and conglomerates) distributed in Northeastern Thailand—Southwestern Laos (Racey et al., 1996). The size of gravel clasts ranges from 2 mm to 3 cm, showing poor sorting (Fig. 6a). The shape analysis reveals that there are two populations of shapes. One is angular to subrounded ($R_k = 0\text{--}0.4$) and the other is rounded to well-rounded ($R_k = 0.4\text{--}1$; Fig. 6b and 6f). Some of the angular clasts preserve rounded surfaces (Fig. 6c), indicating that they were formed by breaking of rounded pebbles. Irregular fractures commonly are observed in all clasts lithologies. In particular, quartzite gravel clasts are most extensively fractured (Fig. 6d and 6e). The bimodal distribution of

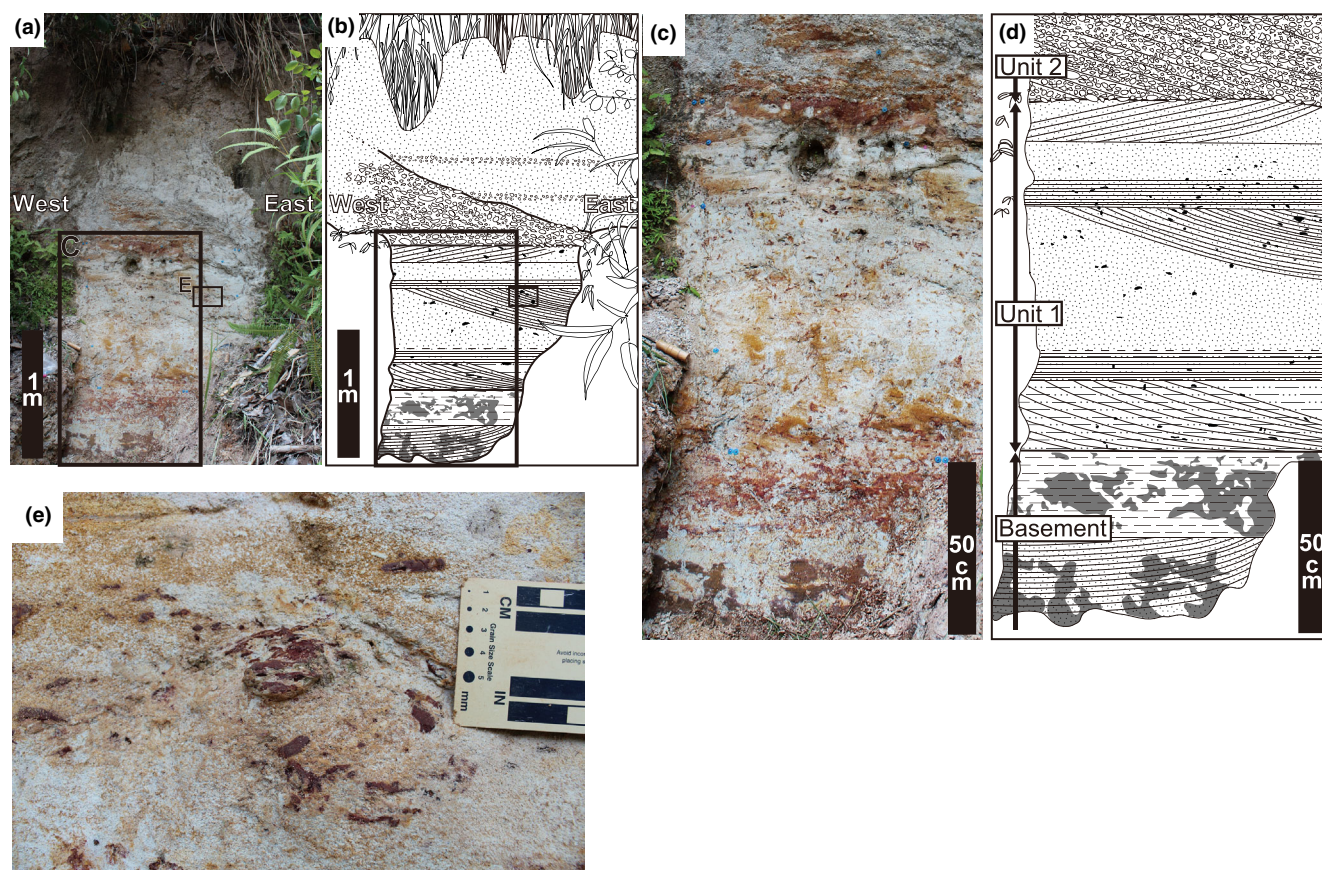


Fig. 5. a and b) A field photograph and its sketch of subsection B at Huai Om. c and d) An enlarged photograph and its sketch of the basement, Units 1 and 2. Unit 1 and the lower part of Unit 2 show cross-stratification. The basement is purplish gray sandstone and red mudstone in ascending order, and both are partly altered to whitish gray in color probably due to weathering. The position of the photograph (c) is indicated with the rectangle in the photograph (a). Legends of the sketches are same as Fig. 3. e) A field photograph of rip-up clasts of the basement red mudstone occurred in Unit 1. The position of the photograph is indicated with a rectangle in the photograph (a). (Color figure can be viewed at wileyonlinelibrary.com.)

roundness of gravel clasts and the presence of fragments of rounded pebbles as well as the occurrence of highly fractured rounded gravel clasts indicate that the clasts in Unit 2 were derived from rounded gravels, some of which were fractured or fragmented. The matrix of Unit 2 is composed mostly of single-crystal quartz with minor amounts of chert, mudstone, and siliceous sandstone fragments of 100–300 μm in diameter. Clay-size grains are rare.

Unit 3 is composed almost exclusively of single-crystal quartz of 100–300 μm in diameter (Fig. S7b). Trace amounts of zircon, olivine, and opaque minerals are also present.

Grain Size Distribution of <2 mm Fraction

The grain size distribution for Unit 1 shows a trimodal distribution: two dominant modes are approximately at 4 μm (clay–very fine silt) and 250 μm (fine–medium sand), respectively, and one minor mode is

approximately at 64 μm (coarse silt–very fine sand), which are similar to the grain size distribution of the weathered basement (Fig. S6). The fraction of the clay–very fine silt could be overestimated due to disaggregation of mudstone fragments during the pretreatment of samples. However, the shape of the grain size distributions seems to be consistent with the results of the thin section observations. As for Unit 2, the grain size distributions are bimodal: The dominant mode is approximately at 250 μm (fine–medium sand), and a minor mode is approximately at 4 μm (clay–very fine silt). These multimodal distributions represent the poor sorting of Units 1 and 2 (Fig. S6).

The grain size distribution for Unit 3 shows a unimodal distribution with the modal diameter of approximately 250 μm (fine–medium sand; Fig. S6). The grain size distribution of Unit 3 is constant throughout the unit, consistent with the massive texture of Unit 3. The standard deviation (as an index of sorting) is

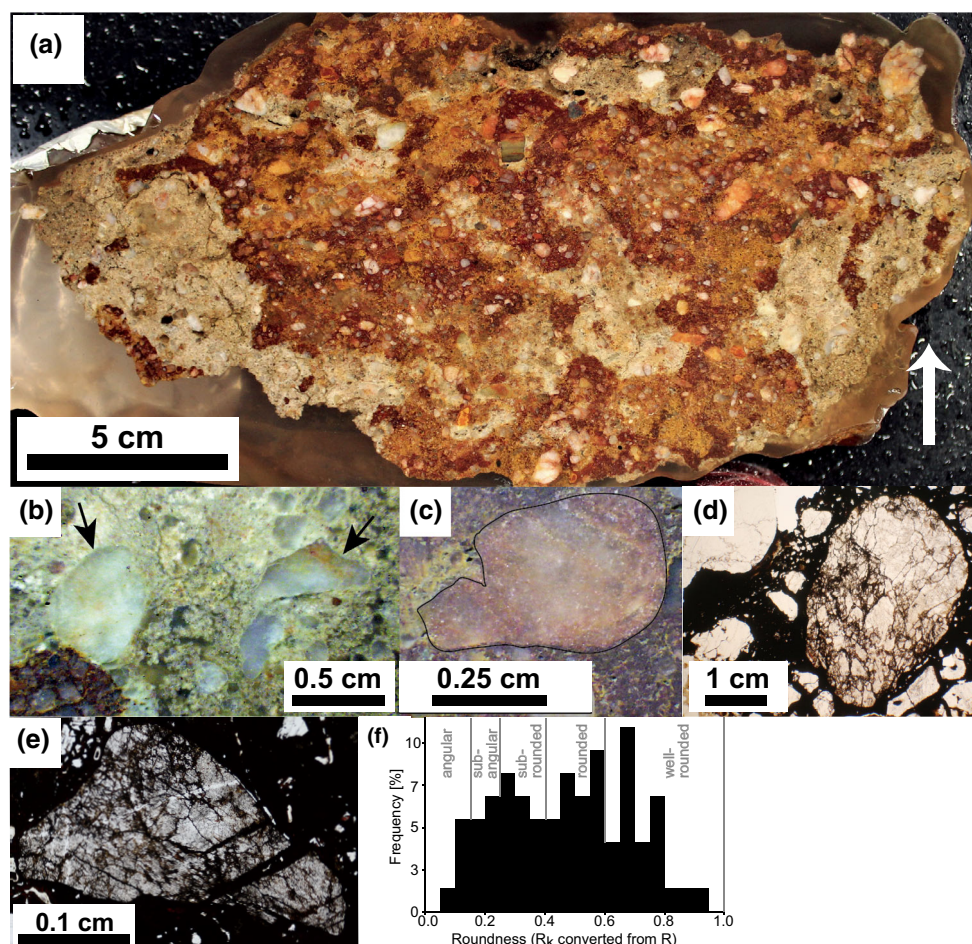


Fig. 6. a) A photograph of the polished slab section of Unit 2. This unit is composed mainly of poorly sorted white quartzite granules to pebbles that are partly cemented by Fe/Mn oxides, which can be seen as red color. The white arrow represents the stratigraphic upper direction. The stratigraphic position of the slab sample is shown in Fig. 3. b) A photograph showing co-occurrence of subangular and well-rounded quartzite gravels in Unit 2. Left is well rounded ($R_k = 0.89$) and right is subangular ($R_k = 0.21$). c) A photograph of broken quartzite gravel in Unit 2 that preserves rounded surface. d and e) Photomicrographs of highly fractured quartzite gravels in Unit 2 (parallel polars). f) A histogram of the roundness index based on the grain shape analysis. There are two populations in the roundness of the gravels: subangular to subrounded and rounded to well rounded. (Color figure can be viewed at wileyonlinelibrary.com.)

1.0–1.3 Φ , indicating that a good sorting is attained during transportation and sedimentation.

Occurrence of the Lamellae in Quartz

Some quartz grains from Units 1–3 have curved and subparallel lamellae (Fig. 7). Some of the lamellae have birefringence different from the host quartz under the optical microscope. These lamellae are 2–7 μm thick, 2–15 μm apart, and occur as a single set per grain. These features are consistent with the characteristics of tectonic deformation lamellae (e.g., French & Koeberl, 2010), and thus, these lamellae are of tectonic origin.

Quartz grains with sharp, planar to subplanar, and parallel lamellae, which are <1–2 μm thick and 2–10 μm

apart, are found throughout Units 1–3 at Huai Om subsection A (Figs. 8–10). These lamellae exhibit no birefringence for any orientation under crossed polarizers indicating that these lamellae are not elongated subgrains. These lamellae mostly occur within sand-sized single crystalline quartz grains of 100–300 μm in diameter. In addition, they also occur in quartzite gravel clasts and quartz in sandstone clasts in Unit 2. Some of the lamellae penetrate through the whole grains (Figs. 8 and 9b), while some lamellae develop in a part of the grains (Figs. 9a and 10). The lamellae commonly occur as a single set per grain, but some quartz grains have multiple sets of lamellae, with up to three sets per grain (Figs. 9a and 10). The results of observations and measurements focusing on this type of lamellae in quartz are described in this section.

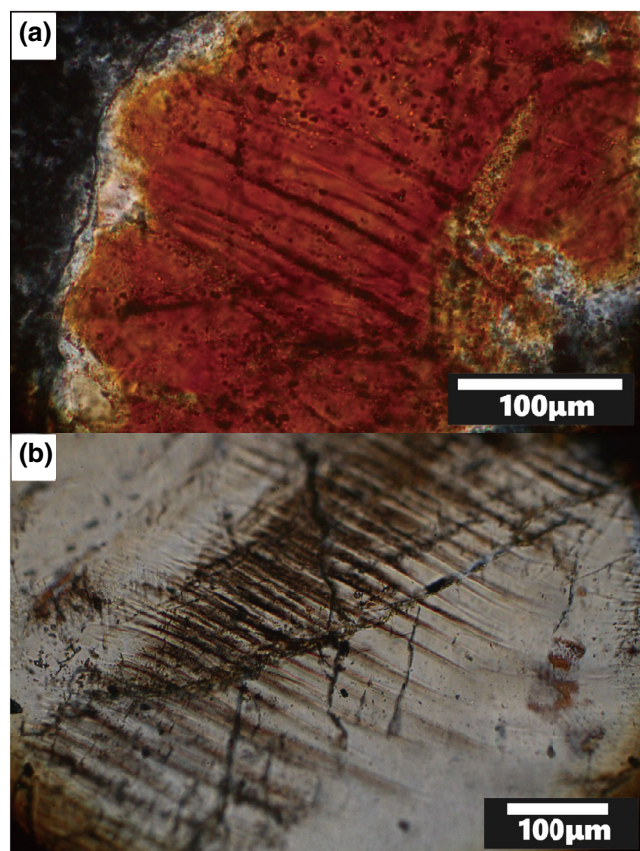


Fig. 7. Examples of typical tectonic deformation lamellae in quartz from the Huai Om section (under crossed polars). a) From Unit 1. b) From Unit 2. These lamellae are thick (2–7 μm), widely spaced (2–15 μm apart), vague, and sinuous, which are different from PDFs in shocked quartz. (Color figure can be viewed at [wileyonlinelibrary.com](https://onlinelibrary.wiley.com/doi/10.1111/j.1365-3113.2021.1000000000000000).)

Of the 125 quartz grains with the lamellae from the Huai Om section, 77.6% (97 grains) have a single set, 21.6% (27 grains) have two sets, and 0.8% (1 grain) display three sets of the lamellae. The average and standard deviation (in parentheses) of the number of sets per grain is 1.23 (0.44; Table S1 in supporting information).

The polar angle distribution of 154 sets of the lamellae in 125 grains measured with the universal stage shows several distinct peaks in frequency (Fig. 11; Fig. S10 in supporting information). In particular, striking peaks occur in 20–30° to the c -axis corresponding to the lower Miller–Bravais indices such as $\omega\{10\bar{1}3\}$, $\pi\{10\bar{1}2\}$, which are typical orientations of PDFs. Most of the measured lamellae sets can be indexed to specific crystallographic orientations, and unindexed planes are less than 10% (Table S1; Fig. 11).

Because the orientation of the a -axis of quartz cannot be identified by optical microscopy, we can only determine the angle to the c -axis, which alone is insufficient for unequivocal comparison of the orientation of the lamellae and that of PDFs. This problem cannot be solved if the quartz grain has only

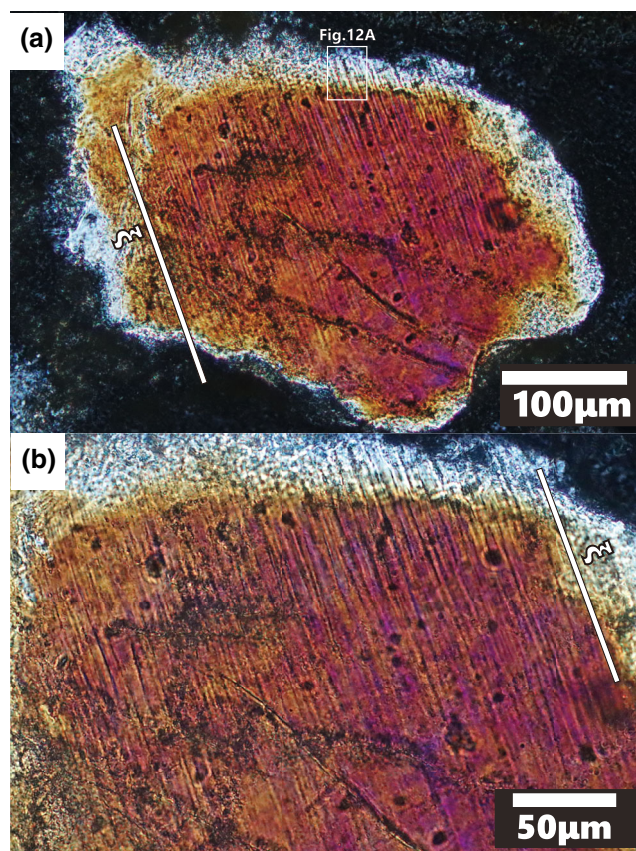


Fig. 8. a) A photomicrograph of an example of PDFs in quartz from the Huai Om section from Unit 1 (sample HO10; crossed polars). The lamellae are thin (<1–2 μm), narrow spaced (2–10 μm apart), sharp, plane, and parallel, which are different from tectonic deformation lamellae. The rectangle indicates the area observed with SEM (see Fig. 12a). b) An enlarged photomicrograph of the same grain in (a). (Color figure can be viewed at [wileyonlinelibrary.com](https://onlinelibrary.wiley.com/doi/10.1111/j.1365-3113.2021.1000000000000000).)

one set of lamellae, although it is possible to see whether the orientations of the lamellae could agree with the orientations of PDFs or not. However, if the grain contains at least two sets of lamellae, the orientation of the lamellae can be reliably tested to be consistent with the orientation of PDFs or not, because there is further information on the angle between the sets of the lamellae in addition to the angle to the c -axis (Langenhorst, 2002; Stöffler & Langenhorst, 1994). Figure 11e shows the distribution of the orientation and indexing results of the lamellae from the Huai Om section which occurred as multiple sets per grain. Even restricted to the lamellae that occurred as multiple sets per grain, their orientations mostly coincide with the specific crystallographic orientations of PDFs, and unindexed planes are less than 10%.

SEM observation of the lamellae in the quartz grains, 201205-1 from Unit 1 (HO10) and 19d-3 from Unit 3 (HO19), indicated that most parts of the

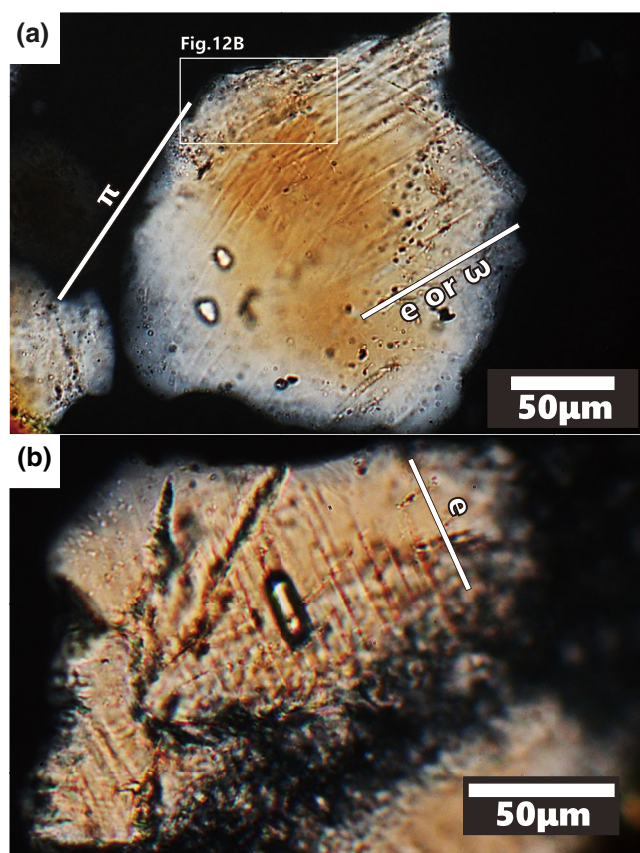


Fig. 9. Photomicrographs of examples of PDFs in quartz from the Huai Om section (crossed polars). a) Intersecting two sets of PDFs found in a quartz grain from Unit 3 (sample HO19). The rectangle indicates the area observed with SEM and TEM (see Fig. 12b and 12c). b) Single set of PDFs in a quartz grain found from Unit 1 (sample HOUnit1_4). (Color figure can be viewed at wileyonlinelibrary.com.)

lamellae occurred as alignment of tiny ($\sim 0.1 \mu\text{m}$ sized) pits (Fig. 12a and 12b). In some parts, the lamellae occurred as a line darker than the host quartz under backscattered electron (BSE) imaging (e.g., the white circled area in Fig. 12a). The apparent thickness and spacing of the lamellae on the thin section surfaces are $0.2\text{--}0.9 \mu\text{m}$ thick and $1.0\text{--}5.9 \mu\text{m}$ apart for the grain 201205-1 (Fig. 12a), and $0.6\text{--}2.4 \mu\text{m}$ thick and $0.8\text{--}3.7 \mu\text{m}$ apart for the grain 19d-3 (Fig. 12b). Because the lamellae in Fig. 12b intersects diagonally to the plane of the thin section, the apparent thickness and spacing of the lamellae in the SEM images are wider than the actual thickness and spacing of the lamellae. Because the angle between the lamellae and the plane of the thin section measured by the universal stage is $37\text{--}40^\circ$, the actual thickness and spacing of the lamellae in Fig. 12b are calculated as $0.4\text{--}1.5 \mu\text{m}$ thick and $0.5\text{--}2.4 \mu\text{m}$ apart, respectively. The lamellae in Fig. 12a intersects the thin section plane almost perpendicularly ($85\text{--}86^\circ$ to the thin section plane). Thus, the difference between the apparent

thickness/spacing and the actual thickness/spacing is negligible for the lamellae in Fig. 12a.

TEM observation of the ultrathin section that was cut perpendicular to the lamella in the grain 19d-3 revealed that the lamella is $1.1 \mu\text{m}$ thick and characterized by a high density of tiny ($\sim 0.1 \mu\text{m}$ in diameter) vugs (Fig. 12c). The orientation of the crystal does not change across the lamella, which is confirmed by undisturbed bend-contours (dark black bands in Fig. 12c). Thus, the lamella in Fig. 12c is not an elongated subgrain.

The abundance of the quartz grains with the lamellae to total quartz grains counted on the three thin sections (HOUnit1-1, HOUnit2-1, HO19) is $2.3\%\text{--}3.6\%$ (Fig. S11 in supporting information). We note that the abundance of the quartz grains with the lamellae counted on the thin sections would be underestimated because some of the lamellae, developing only in a part of the grains, may not appear on a thin section plane unless the lamellae coincidentally are intersected by the thin section plane.

DISCUSSION

Identification of PDFs in Shocked Quartz

In this section, the characteristics of the lamellae described in [Occurrence of the Lamellae in Quartz](#) section are compared with the criteria for identifying PDFs described in [Criteria to Identify PDFs in Quartz](#) section.

1. *Spacing of lamellae:* The spacing of the lamellae in quartz grains from the Huai Om section is $2\text{--}10 \mu\text{m}$ under the optical microscope (Figs. 8 and 9). The SEM images of the lamellae show that the spacing is $0.5\text{--}5.9 \mu\text{m}$ for high resolution images (Fig. 12a and 12b). The spacing of the lamellae is in the range of that of PDFs in shocked quartz ($<2\text{--}10 \mu\text{m}$ under optical microscopy and $<1\text{--}4 \mu\text{m}$ under TEM; e.g., Ashworth & Schneider, 1985; French & Koeberl, 2010; Stöffler & Langenhorst, 1994).
2. *Thickness of lamellae:* The thickness of the lamellae from the Huai Om section is $<1\text{--}2 \mu\text{m}$ under the optical microscope and $0.2\text{--}1.5 \mu\text{m}$ in SEM/TEM images (Fig. 12). Although the thickness of some of the lamellae is slightly thicker than that of typical PDFs ($<1 \mu\text{m}$; French & Koeberl, 2010; Goltrant et al., 1992; Grieve et al., 1996), the thickness is still in the range of that of PDFs previously reported ($2 \mu\text{m}$ as a maximum; Hough et al., 2003; Stöffler & Langenhorst, 1994) and thinner than that of tectonic deformation lamellae in quartz ($>2 \mu\text{m}$; Drury, 1993; French & Koeberl, 2010; McLaren & Hobbs, 1972).

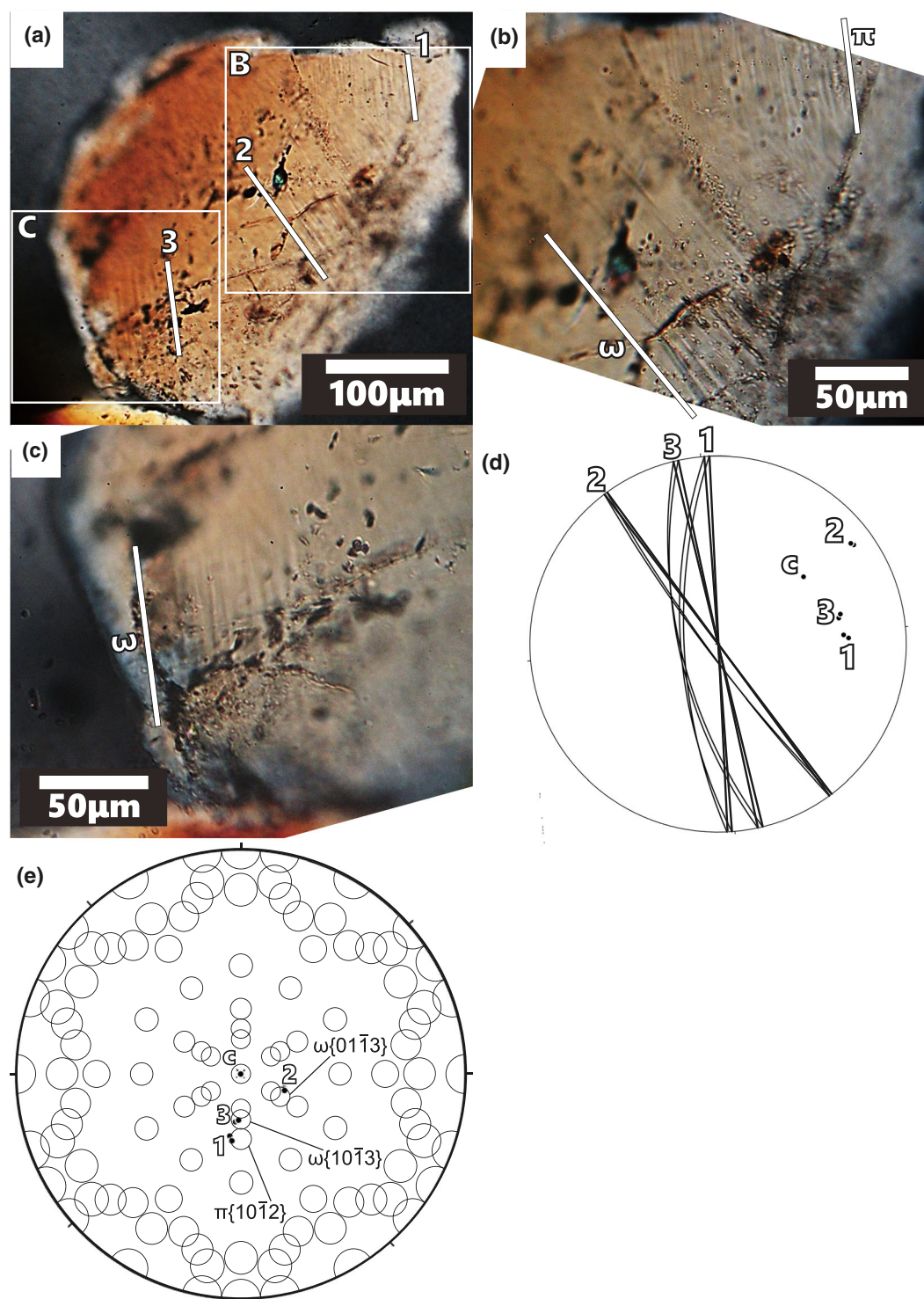


Fig. 10. a) Photomicrograph of a shocked quartz grain with three sets of PDFs found from the Huai Om section Unit 3 (sample HO15; crossed polars). b and c) Enlarged photomicrographs of the same grain in (a) showing each set of the lamellae. d) Measured orientations of the PDFs and quartz c -axis plotted in the stereonet (equal-angle projection). Each orientation was measured twice. e) Stereoplot of orientations of poles to PDFs measured in the quartz grain shown in (a). Template shows low Miller indices in quartz according to von Engelhardt and Bertsch (1969), with additional indices as suggested by Ferrière et al. (2009). Each crystallographic orientation is depicted as 5° circles including measurement error. Poles to the PDFs are located near the $\omega\{10\bar{1}3\}/\{01\bar{1}3\}$ planes and $\pi\{10\bar{1}2\}$ plane, showing that the orientations of these lamellae are crystallographically controlled. (Color figure can be viewed at wileyonlinelibrary.com.)

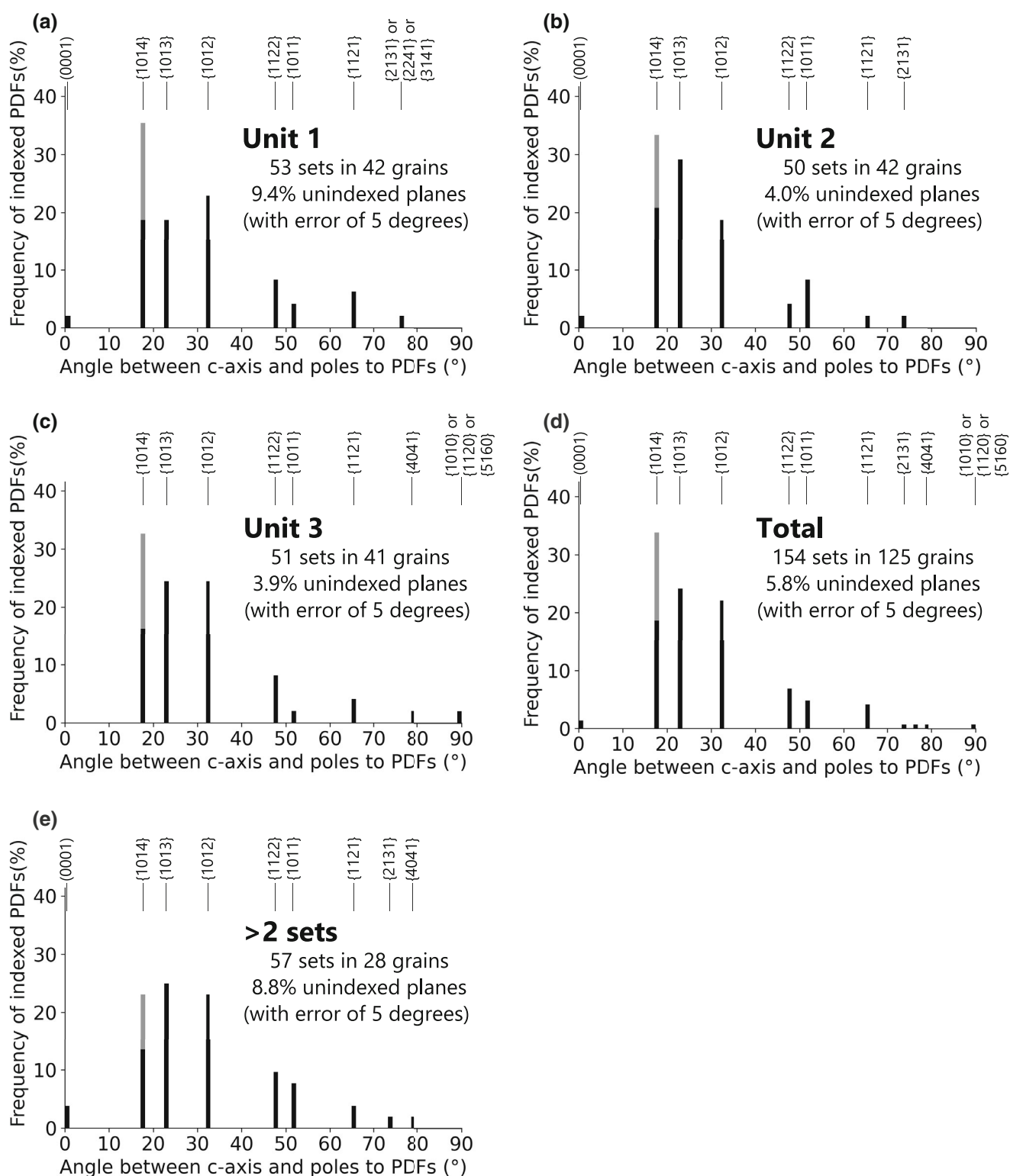


Fig. 11. Histograms of absolute frequency percent of indexed PDFs in quartz grains from the Huai Om section for Unit 1 (a), Unit 2 (b), and Unit 3 (c), for all measured grains from Units 1–3 (d), and for grains with multiple sets from Units 1–3 (e). Note that the total number of values was recalculated to 100% without unindexed PDF orientations. The frequency distributions of the measured angles between the quartz *c*-axis and the pole of the lamellae are shown in Fig. S10 in Appendix S1.

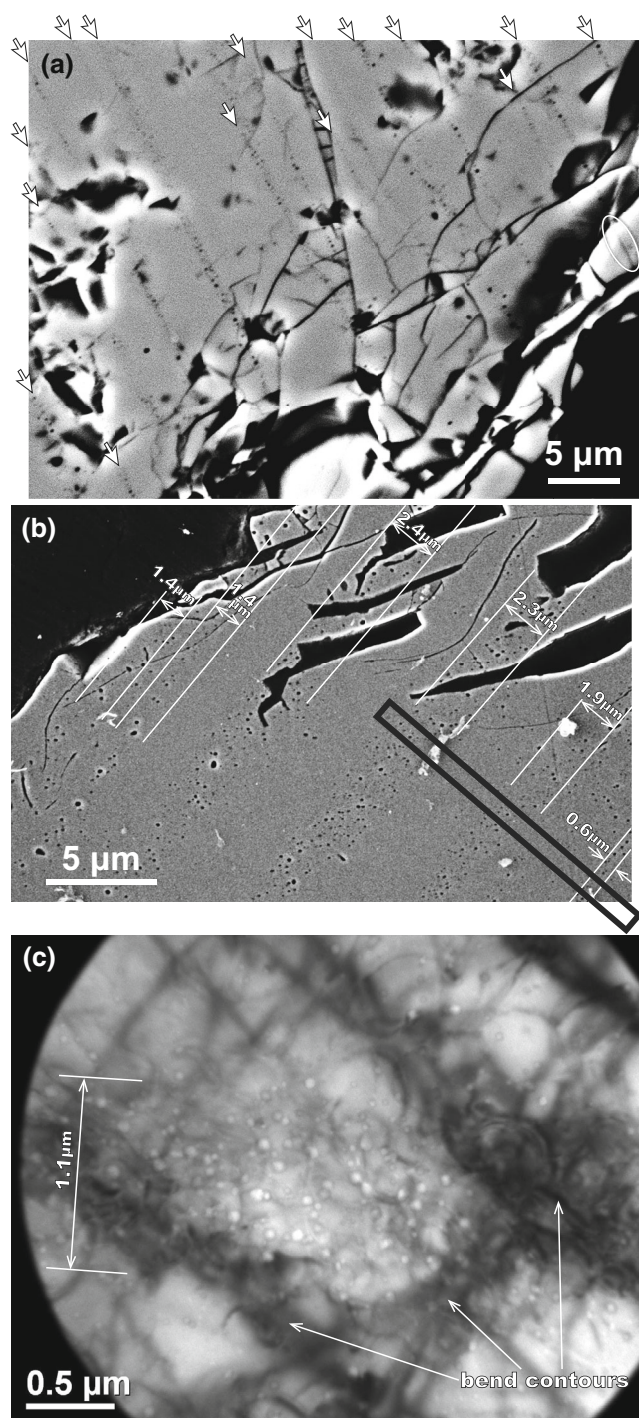


Fig. 12. a) SEM-BSE image of a quartz grain with PDFs from Unit 1 at Huai Om subsection A (the same grain as in Fig. 8). The area of the image is indicated in Fig. 8a. Each plane in the lamellae is indicated by white arrows. Most parts of the lamellae are observed as alignment of small ($\sim 0.1 \mu\text{m}$ sized) pits. In some parts, the lamellae occurred as a line darker than the host quartz as shown in the white circled area. The thickness and spacing of the lamellae are $0.2\text{--}0.9 \mu\text{m}$ thick and $1.0\text{--}5.9 \mu\text{m}$ apart. b) SEM-BSE image of one quartz grain with PDFs from Unit 3 (the same grain as in Fig. 9a). White auxiliary lines are showing the orientation and apparent thickness of the lamella. Since the lamella intersects diagonally ($37\text{--}40^\circ$) to the plane of the thin section, the apparent thickness and spacing of the lamella in the SEM image are wider than the actual thickness and spacing. The actual thickness and spacing of the lamella are calculated as $0.4\text{--}1.5 \mu\text{m}$ thick and $0.5\text{--}2.4 \mu\text{m}$ apart. The rectangle at the bottom-right indicates the area to prepare an ultrathin section for TEM. c) Bright-field TEM images from the area containing PDF. The PDF (E–W orientation in the image) is $1.1 \mu\text{m}$ thick and composed of tiny vugs of $\sim 0.1 \mu\text{m}$ in diameter. The continuous bend contours indicate that the orientation of the crystal does not change across the lamellae.

is different from the broad bell-shaped distribution of the orientation of tectonic deformation lamellae in quartz (e.g., French & Koeberl, 2010; von Engelhardt and Bertsch 1969).

3. *Orientation of lamellae:* Based on the results of the measurement of orientations of the lamellae from the Huai Om section, it is clear that the orientations of the lamellae are crystallographically controlled and coincide with the orientations of PDFs in quartz (Fig. 11; Fig. S10). The shape of the histogram of the orientation of the lamellae clearly

4. *Number of sets of lamellae per grain:* The average and standard deviation (in parentheses) of the number of sets per grain for the lamellae in quartz from the Huai Om section is 1.23 (0.44). The average number of PDF sets per quartz grain from the K/Pg boundary deposits proximal to the Chicxulub crater (in Cuba and Gulf of Mexico) is 1.2 (0.4)–1.7 (0.9) (Nakano et al., 2008). The average number of sets per grain for the lamellae in quartz from Huai Om is comparable to that from the K/Pg boundary deposits proximal to the Chicxulub crater.

5. *Component of lamellae:* The occurrence of the lamellae on the SEM/TEM images is similar to the decorated type PDFs, which are composed of alignment of tiny vugs (Goltrant et al., 1991; Grieve et al., 1996), and clearly different from tectonic deformation lamellae, which are elongated subgrains associated with subgrain walls, across which the orientation of the crystal changes slightly (Cordier et al., 1994; Langenhorst & Deutsch, 1996; Vernooij & Langenhorst, 2005) (Fig. 12). It has been reported that nondecorated type PDFs can be observed as lines darker than the host quartz under SEM-BSE images (e.g., Fazio et al., 2014; Kowitz et al., 2016). Because the decorated type PDFs are formed by thermal alteration of nondecorated type PDFs (Goltrant et al., 1991; Grieve et al., 1996), the

parts of the lamellae observed as dark lines in the SEM-BSE image (Fig. 12a) are possibly unaltered remains of nondecorated type PDFs.

The characteristics of the lamellae in quartz from the Huai Om section satisfy the criteria (1)–(5) for identifying PDFs. However, there are some characteristics of the lamellae which are different from typical PDFs in quartz. The first characteristic is that some of the lamellae are slightly thicker ($>1\ \mu\text{m}$) when compared with typical PDFs ($<1\ \mu\text{m}$; e.g., French & Koeberl, 2010). This fact may be explained by broadening of PDFs due to partial amorphization of quartz (Langenhorst, 1994). Langenhorst (1994) proposed a model of the formation of diaplectic glass, in which the diaplectic glass is formed by broadening of amorphous lamellae (PDFs), based on TEM observations of experimentally shock-deformed quartz and temperature calculations. In this model, the amorphization of quartz crystal starts from areas adjacent to PDFs, and finally, the entire quartz grain becomes amorphous glass as the degree of shock deformation increases, because the shock temperature is distinctly higher in amorphous PDFs than in crystalline quartz areas (Langenhorst, 1994). It is also known that if porous sandstone is a target rock, the shock temperature is more likely to be raised higher than reached within crystalline target rock at the same shock pressure (e.g., Kieffer, 1971; Kowitz et al., 2016; Stöffler et al., 2018). Because the target rock of the AATE is considered to be Mesozoic sandstone (e.g., Blum et al., 1992; Glass & Koeberl, 2006) and Quaternary basalt (Sieh et al., 2020), and quartz grains are considered to have been derived from Mesozoic sandstone, the high shock temperature in the porous sandstone could have caused the broadening of the PDFs to occur efficiently, resulting in the formation of thicker PDFs.

The other characteristic that differs from typical PDFs in quartz with regard to the lamellae from the Huai Om section is the occurrence of the lamellae oriented in $\pi\{10\bar{1}2\}$ as a single set per grain. The number of PDF sets per grain increases with increasing shock pressure that the host quartz has experienced (e.g., Stöffler & Langenhorst, 1994). It is known that PDFs oriented in $\pi\{10\bar{1}2\}$ are formed by shock pressures larger than 20 GPa (e.g., Stöffler & Langenhorst, 1994). Thus, it is expected that PDFs oriented in $\pi\{10\bar{1}2\}$ occur as multiple sets in a quartz grain. However, most lamellae in quartz grains from the Huai Om section occur as a single set despite a high amount of the lamellae oriented in $\pi\{10\bar{1}2\}$ (Fig. 11; Table S1). This problem also may be attributable to the type of target rock. The shock deformation experiments of quartz and observations of shocked quartz in impact structures

mostly have been conducted on single-crystal quartz or dense crystalline targets. The occurrence (orientations and number of sets) of PDFs in porous sedimentary targets is poorly studied (e.g., Kowitz et al., 2016). Shock deformation experiments have been conducted on porous sandstone targets, but the occurrence of PDFs has not been examined in detail (e.g., Kenkmann et al., 2018; Kowitz et al., 2016; Mansfeld et al., 2017). Observations of PDFs from natural impact craters formed on porous sedimentary targets are also very limited and only several examples are reported (Cox et al., 2019; Folco et al., 2018; French et al., 1974, 2004; Kieffer, 1971; Reimold et al., 2019). It has been pointed out that the orientations of PDFs in the porous sandstone targets such as BP and Oasis craters and Rock Elm crater tend to show distribution different from that of the typical PDFs formed in crystalline targets (French et al., 1974, 2004). According to the data of Cox et al. (2019) and Reimold et al. (2019), quartz grains with single sets of PDFs oriented in $\pi\{10\bar{1}2\}$ are present in porous sandstone targets in Yallalie crater and Cerro do Jarau crater, although the number of the measurement was small (only nine sets in six grains and ten sets in nine grains were measured with respect to their orientation, respectively).

In summary, the characteristics of the lamellae in quartz from the Huai Om section, such as thickness, spacing, number of sets per grain, orientation, and component, satisfy the criteria (1)–(5) in general and support the assertion that the lamellae are PDFs. Thus, the quartz grains with the lamellae from the Huai Om section are identified as shocked quartz grains. Although there are some characteristics of the lamellae that are different from typical PDFs previously reported, they are probably attributable to the type of target rock that is most likely a porous sandstone.

Identification of the Ejecta Deposit of AATE at Huai Om Section

The presence of quartz grains with PDFs ($>2\text{--}3\%$ of the total quartz grains counted) throughout Units 1–3 suggests that the Quaternary sequence of Units 1–3 at the Huai Om section is likely representing a single sequence of the ejecta deposit.

There are no definitive criteria for the abundance of shocked quartz required to identify ejecta deposits. Retallack et al. (1998) interpreted the possible shocked quartz grains from the Permian–Triassic boundary layer in Australia and Antarctica as a result of redeposition from older impact structures, or ejecta deposits, based on the low abundance of the possible shocked quartz ($<0.2\%$). Van Hoesel et al. (2015) interpreted shocked quartz from the Allerød–Younger Dryas boundary in

the Netherlands as redeposited mainly based on the low abundance ($<0.02\%$). The abundance of shocked quartz in ejecta deposits of the K/Pg impact event varies from 5% to 40% (e.g., Chang et al., 2018; Nakano et al., 2008). The abundance of shocked quartz in the sequence at the Huai Om section ($>2\text{--}3\%$) is higher than that considered as redeposited ejecta materials, and closer to the lower abundance in K/Pg ejecta deposits.

The continuous occurrence of shocked quartz throughout the Quaternary sequence at Huai Om indicates that Units 1–3 represent the ejecta deposit. However, a question of its depositional age remains. Recently, Tada et al. (2020) reported the detailed occurrence of 331 fragments of an MN tektite from the upper part of Unit 2 at HO06 section located 15 km to the southwest of the Huai Om section. The occurrence of the tektite fragments concentrated in a small area as well as their angular shape, size distribution, the restoration of larger tektite fragments into one ellipsoidal MN tektite mass, and similar chemical composition of the fragments indicate that these tektite fragments originally formed one large (~ 30 to 40 cm sized) MN tektite, which was buried immediately after fragmentation (Tada et al., 2020). Thus, they consider that these tektite fragments were formed in situ at the time of landing of a large MN tektite on the ground after traveling along the ballistic trajectory. The in situ occurrence of the fragments of MN tektite at HO06 section in addition to the presence of the shocked quartz with PDFs at the Huai Om section strongly indicates that Unit 2 (“laterite” layer) and underlying Unit 1 represent the ejecta deposit formed by the AATE. The fact that tektites have been found from the upper part, or at the top, of the “laterite” layer at several sites in northeastern Thailand, southern Laos, and central Vietnam (Barnes & Pitakpaivan, 1962; Fiske et al., 1996, 1999; Schnetzler & McHone, 1996; Songtham et al., 2011, 2012; Tamura, 1992; Wasson et al., 1995) indicates that the ejecta deposit is distributed widely in the eastern part of Indochina.

Implication for the Depositional Process of the Ejecta Deposit

The presence of the three distinct lithostratigraphic units in the shocked quartz-bearing Quaternary sequence, which have different sedimentary structure, color, grain size, and grain composition, indicates that each unit has been formed by different depositional processes.

The presence of clasts derived from the underlying weathered Mesozoic basement rocks in Unit 1 (Fig. 5e), as well as similarities in grain composition and grain size distribution between Unit 1 and the weathered Mesozoic sandstone basement (Fig. S6), suggests the

reworking origin of Unit 1 from the underlying weathered basement. This occurrence of the reworked materials in this unit, as well as the presence of cross-lamination, suggests that Unit 1 was deposited under the influence of an erosive flow. The very poorly sorted nature of this unit characterized by the trimodal grain size distribution (Fig. S6) suggests that this unit has not been sorted during transportation, thus implies rapid deposition. Frequent changes in the apparent dip direction of the cross-lamination at subsection B (Fig. 3) possibly reflect frequent changes in the paleocurrent direction of the local flow. However, a possibility remains that the cross-lamination is trough type because we did not examine the types of the cross-lamination in three-dimensional sections.

It has been suggested that when an asteroid hits a planet with an atmosphere, strong winds should blow laterally from the impact point owing to expansion of vapor plume into the ambient atmosphere (e.g., Quintana et al., 2018; Schultz, 1992; Schultz & Quintana, 2017). The studies of proximal ejecta deposits of the Chicxulub impact structure found in the Albion formation in Mexico and Belize revealed that a granular silt layer containing spherules lies between the basement dolomite and coarse very poorly sorted diamictite layer (Ocampo et al., 1996; Pope et al., 1999). Therefore, it has been proposed that the deposition of fine ejecta due to strong lateral wind caused by expansion of vapor plume would have occurred before the deposition of the ejecta curtain gravels at this site (Ocampo et al., 1996; Pope et al., 1999). Based on these arguments, Unit 1 observed at the Huai Om section may also have been deposited by the impact-induced wind, which occurred immediately after the initial air blast that stripped away surficial vegetation and soils covering the weathered basements around the impact point.

Unit 2 is a tektite-bearing, poorly sorted gravel layer containing silt to gravel (up to 3 cm) sized grains. As mentioned previously, the clasts in Unit 2 are a mixture of rounded gravels and angular gravels probably formed by fracturing of rounded gravels. The poorly sorted nature and the occurrence of the fragmented angular gravels indicate rapid deposition of this unit. In addition, the occurrence of in situ MN tektite fragments (Tada et al., 2020), which is a melted crustal rock ejected from the impact point, suggests that this unit represents the ejecta curtain deposit.

Unit 3 is a well-sorted massive fine to medium sand layer. Although the boundary between Units 2 and 3 is relatively sharp, there is no evidence of erosion at the base of Unit 3. The good sorting, nearly constant fine to medium grain size, and lack of sedimentary structures suggestive of lateral flow imply that Unit 3 was deposited as air-fall rather than by lateral flow.

Consequently, the suggested interpretation on the origin of Units 1–3 is as follows: rework of the local basement rocks by the impact generated vapor wind (Unit 1), followed by deposition of the ejecta curtain gravels including gravels and MN tektites (Unit 2), and, finally, the deposition of fine fallout ejecta (Unit 3).

Based on this interpretation, further investigation of the lateral distribution of Units 1–3, especially of Unit 2, in terms of its thickness, grain size, and grain composition could provide information about the location, magnitude, and target rocks of the AATE.

CONCLUSIONS

In this paper, we report on the detailed lithostratigraphy of the Quaternary sequence at the Huai Om section in northeastern Thailand. Shocked quartz grains with PDFs were discovered throughout the Quaternary sequence. PDFs were confirmed by their thickness, spacing, and the measurement of their orientation with a universal stage microscope, as well as SEM and TEM observations of the lamellae, showing that the lamellae occur as alignment of tiny ($\sim 0.1 \mu\text{m}$ size) vugs similar to decorated PDFs (Goltrant et al., 1991; Grieve et al., 1996). Although there are some characteristics of the lamellae with regard to their thickness and the polar angle distribution that are different from typical PDFs previously reported, they are probably attributable to the type of target rock, which most likely was a porous sandstone.

The shocked quartz-bearing sequence can be divided into three lithostratigraphic units (Units 1–3 in ascending order) based on the difference in the sedimentary structure, color, grain size, and grain composition, indicating that each unit was formed by different depositional processes within one impact event.

Unit 1 is composed of decimeter-scale alterations of whitish-gray silt and fine sand layers that contain various amounts of rip-up clasts of the basement mudstone and occasionally show cross-lamination. Unit 2 is a reddish-brown sandy granule to pebble layer that contains fractured angular gravels. Unit 3 is composed of a whitish to light brownish-gray massive fine to medium sand that is well sorted compared with lower Units 1 and 2.

The presence of the shocked quartz grains throughout Units 1–3 in addition to the occurrence of in situ fragments of an MN tektite from the upper part of Unit 2 (Tada et al., 2020) is diagnostic evidence showing that the Quaternary deposit (Units 1–3) in this area is the proximal ejecta deposit formed by the Australasian Tektite Event.

Based on lithological and sedimentological evidence, Unit 1 is considered as having been deposited by a flow

loaded with fine ejecta grains, possibly induced by the lateral wind of vapor plume expansion, Unit 2 is considered as representing ejecta curtain gravels, and Unit 3 is considered to represent fallout ejecta.

The results of this study provide lithostratigraphic criteria to help identify the proximal ejecta deposit of this impact event that makes it possible to investigate their lateral distribution in the field. Further investigation of the lateral distribution especially of Unit 2 (ejecta curtain deposit) in terms of its thickness, grain size, and grain composition could provide information about the location, magnitude, and target rocks of the Australasian Tektite Event.

Acknowledgments—The extensive comments by Dr. C. Koeberl significantly contributed to improving the manuscript. We also greatly thank Dr. C. Alwmark and the anonymous reviewer for their helpful comments on the previous versions of the manuscript, which greatly improved the manuscript. We are grateful to P. Jintasakul, the director of Khorat Fossil Museum, and P. Singhwachiraworakul for their hospitality during the field survey. We are much obliged to W. Tarora of the University of Tokyo who conducted the sample preparation with FIB for TEM observation. We are grateful to Dr. H. Ono and Dr. T. Arai of the Chiba Institute of Technology for their help during the SEM observations. We sincerely thank Dr. S. Takahashi, Dr. S. Muto, and K. Yoshizawa of the University of Tokyo, and Dr. K. Kurosawa of the Chiba Institute of Technology for valuable discussions. We also thank Dr. H. Tuffen for his kind help during T. Tada's visit to Lancaster University. This study was supported by the Japan Society for the Promotion of Science (JSPS) KAKENHI Fostering Joint International Research (B) 18KK0092 (2018–2021) to R. Tada, and the Fujiwara Natural History Foundation Grant in 2016, Graduate Research Abroad Program (GRASP) 2019 of the University of Tokyo, and Grant-in-aid for JSPS Research Fellow Number 19J13252 awarded to T. Tada. P. A. Carling held a Leverhulme Emeritus Fellowship—2016–2018—which directly supported the project.

Data Availability Statement—The data that support the findings of this study are available from the corresponding author upon reasonable request.

Editorial Handling—Dr. Christian Koeberl

REFERENCES

- Abramoff, M. D., Magalhães, P. J., and Ram, S. J. 2004. Image Processing with ImageJ. *Biophotonics International* 11: 36–42.

- Alexopoulos, J. S., Grieve, R. A. F., and Robertson, R. B. 1988. Microscopic Lamellar Deformation Features in Quartz: Discriminative Characteristics of Shock-Generated Varieties. *Geology* 16: 796–9. [https://doi.org/10.1130/0091-7613\(1988\)016<0796:MLDFIQ>2.3.CO;2](https://doi.org/10.1130/0091-7613(1988)016<0796:MLDFIQ>2.3.CO;2).
- Allmendinger, R. W., Cardozo, N., and Fisher, D. 2011. *Structural Geology Algorithms: Vectors and Tensors*. New York: Cambridge University Press.
- Alvarez, L. W., Alvarez, W., Asaro, F., and Michel, H. V. 1980. Extraterrestrial Cause for the Cretaceous-Tertiary Extinction. *Science* 208: 1095–108. <https://doi.org/10.1126/science.208.4448.1095>.
- Ashworth, J. R., and Schneider, H. 1985. Deformation and Transformation in Experimentally Shock-Loaded Quartz. *Physics and Chemistry of Minerals* 11: 241–9. <https://doi.org/10.1007/BF00307401>.
- Barnes, V. E., and Pitakpaivan, K. 1962. Origin of Indochinite Tektites. *Proceedings of the National Academy of Sciences of the United States of America* 48: 947–55. <https://doi.org/10.1073/pnas.48.6.947>.
- Blum, J. D., Papanastassiou, D. A., Koeberl, C., and Wasserburg, G. J. 1992. Neodymium and Strontium Isotopic Study of Australasian Tektites: New Constraints on the Provenance and Age of Target Materials. *Geochimica et Cosmochimica Acta* 56: 483–92. [https://doi.org/10.1016/0016-7037\(92\)90146-A](https://doi.org/10.1016/0016-7037(92)90146-A).
- Campanale, F., Mugnaioli, E., Folco, L., Gemmi, M., Lee, M. R., Daly, L., and Glass, B. P. 2019. Evidence for Subsolidus Quartz-Coesite Transformation in Impact Ejecta from the Australasian Tektite Strewn Field. *Geochimica et Cosmochimica Acta* 264: 105–17. <https://doi.org/10.1016/j.gca.2019.08.014>.
- Cardozo, N., and Allmendinger, R. W. 2013. Spherical Projections with OSX Stereonet. *Computers and Geosciences* 51: 193–205. [10.1016/j.cageo.2012.07.021](https://doi.org/10.1016/j.cageo.2012.07.021).
- Chang, Y., Goto, K., Sekine, Y., and Tajika, E. 2018. Depositional Processes of Impactites from the YAX-1 Drill Core in the Chicxulub Impact Structure Inferred from Vertical Profiles of PDF Orientations and Grain Size Distributions of Shocked Quartz. *Meteoritics & Planetary Science* 53: 1323–40. <https://doi.org/10.1111/maps.13082>.
- Chao, E. C. T. 1967. Shock Effects in Certain Rock-Forming Minerals. *Science* 156: 192–202. <https://doi.org/10.1126/science.156.3772.192>.
- Christie, J. M., Griggs, D. T., and Carter, N. L. 1964. Experimental Evidence of Basal Slip in Quartz. *The Journal of Geology* 72: 734–56. <https://doi.org/10.1086/627030>.
- Cordier, P., Vrána, S., and Doukhan, J. C. 1994. Shock Metamorphism in Quartz at Sevetin and Susice (Bohemia)? A TEM Investigation. *Meteoritics* 29: 98–9. <https://doi.org/10.1111/j.1945-5100.1994.tb00660.x>.
- Cox, M. A., Cavosie, A. J., Ferrière, L., Timms, N. E., Bland, P. A., Miljković, K., Erickson, T. M., and Hess, B. 2019. Shocked Quartz in Polymict Impact Breccia from the Upper Cretaceous Yallalie Impact Structure in Western Australia. *Meteoritics & Planetary Science* 54: 621–37. <https://doi.org/10.1111/maps.13238>.
- Drury, M. R. 1993. Deformation Lamellae in Metals and Minerals. In *Defects and Processes in the Solid State: Geoscience Applications*, edited by J. N. Boland, and J. D. Fitz Gerald, 195–212. Amsterdam: Elsevier.
- Fazio, A., Folco, L., D'Orazio, M., Frezzotti, M. L., and Cordier, C. 2014. Shock Metamorphism and Impact Melting in Small Impact Craters on Earth: Evidence from Kamil Crater, Egypt. *Meteoritics & Planetary Science* 49: 2175–200. <https://doi.org/10.1111/maps.12385>.
- Ferrière, L., Morrow, J. R., Amgaa, T., and Koeberl, C. 2009. Systematic Study of Universal-Stage Measurements of Planar Deformation Features in Shocked Quartz: Implications for Statistical Significance and Representation of Results. *Meteoritics & Planetary Science* 44: 925–40. <https://doi.org/10.1111/j.1945-5100.2009.tb00778.x>.
- Fiske, P. S., Putthapiban, P., and Wasson, J. 1996. Excavation and Analysis of Layered Tektites from Northeast Thailand: Results of 1994 Field Expedition. *Meteoritics & Planetary Science* 31: 36–41. <https://doi.org/10.1111/j.1945-5100.1996.tb02050.x>.
- Fiske, P. S., Schnetzler, C., McHone, J., and Kham, K. 1999. Layered Tektites of Southeast Asia: Field Studies in Central Laos and Vietnam. *Meteoritics & Planetary Science* 34: 757–61. <https://doi.org/10.1111/j.1945-5100.1999.tb01388.x>.
- Folco, L., Bigazzi, G., Orazio, M. D., and Balestrieri, M. L. 2011. Fission Track Age of Transantarctic Mountain Microtektites. *Geochimica et Cosmochimica Acta* 75: 2356–60. <https://doi.org/10.1016/j.gca.2011.02.014>.
- Folco, L., D'Orazio, M., Gemelli, M., and Rochette, P. 2016. Stretching out the Australasian Microtektite Strewn Field in Victoria Land Transantarctic Mountains. *Polar Science* 10: 147–59. <https://doi.org/10.1016/j.polar.2016.02.004>.
- Folco, L., Mugnaioli, E., Gemelli, M., Masotta, M., and Campanale, F. 2018. Direct Quartz-Coesite Transformation in Shocked Porous Sandstone from Kamil Crater (Egypt). *Geology* 46: 739–42. <https://doi.org/10.1130/G45116.1>.
- Folco, L., Perchiazzi, N., Orazio, M. D., Frezzotti, M. L., Glass, B. P., Rochette, P., Nazionale, M., et al. 2010. Shocked Quartz and Other Mineral Inclusions in Australasian Microtektites. *Geology* 38: 211–4. <https://doi.org/10.1130/G30512.1>.
- French, B. M., Cordua, W. S., and Plescia, J. B. 2004. The Rock Elm Meteorite Impact Structure, Wisconsin: Geology and Shock-Metamorphic Effects in Quartz. *Bulletin of the Geological Society of America* 116: 200–18. <https://doi.org/10.1130/B25207.1>.
- French, B. M., and Koeberl, C. 2010. The Convincing Identification of Terrestrial Meteorite Impact Structures: What Works, What Doesn't, and Why. *Earth-Science Reviews* 98: 123–70. <https://doi.org/10.1016/j.earscirev.2009.10.009>.
- French, B. M., Underwood, J. R., and Edward, P. F. 1974. Shock-Metamorphic Features in Two Meteorite Impact Structures, Southeastern Libya. *Bulletin of the Geological Society of America* 85: 1425–8. [https://doi.org/10.1130/0016-7606\(1974\)85<1425:SFITMI>2.0.CO;2](https://doi.org/10.1130/0016-7606(1974)85<1425:SFITMI>2.0.CO;2).
- Glass, B. P., and Koeberl, C. 2006. Australasian Microtektites and Associated Impact Ejecta in the South China Sea and the Middle Pleistocene Supereruption of Toba. *Meteoritics & Planetary Science* 41: 305–26. <https://doi.org/10.1111/j.1945-5100.2006.tb00211.x>.
- Glass, B. P., and Pizzuto, J. E. 1994. Geographic Variation in Australasian Microtektite Concentrations: Implications Concerning the Location and Size of the Source Crater. *Journal of Geophysical Research* 99: 19075–81. <https://doi.org/10.1029/94JE01866>.
- Glass, B. P., and Wu, J. 1993. Coesite and Shocked Quartz Discovered in the Australasian and North American Microtektite Layers. *Geology* 21: 435–8. [https://doi.org/10.1130/0091-7613\(1993\)021<0435:CASQDI>2.3.CO;2](https://doi.org/10.1130/0091-7613(1993)021<0435:CASQDI>2.3.CO;2).

- Glikson, A. 2004. Comment on "Bedout: A Possible End-Permian Impact Crater Offshore of Northwestern Australia." *Science* 306: 613–3. <https://doi.org/10.1126/science.1100404>.
- Goltrant, O., Cordier, P., and Doukhan, J. C. 1991. Planar Deformation Features in Shocked Quartz: a Transmission Electron Microscopy Investigation. *Earth and Planetary Science Letters* 106: 103–15. [https://doi.org/10.1016/0012-821X\(91\)90066-Q](https://doi.org/10.1016/0012-821X(91)90066-Q).
- Goltrant, O., Leroux, H., Doukhan, J. C., and Cordier, P. 1992. Formation Mechanisms of Planar Deformation Features in Naturally Shocked Quartz. *Physics of the Earth and Planetary Interiors* 74: 219–40. [https://doi.org/10.1016/0031-9201\(92\)90012-K](https://doi.org/10.1016/0031-9201(92)90012-K).
- Gratz, A. J., Fiesler, D. K., and Bohor, B. F. 1996. Distinguishing Shocked from Tectonically Deformed Quartz by the Use of the SEM and Chemical Etching. *Earth and Planetary Science Letters* 142: 513–21. [https://doi.org/10.1016/0012-821X\(96\)00099-4](https://doi.org/10.1016/0012-821X(96)00099-4).
- Gratz, A. J., Nellis, W. J., Christie, J. M., Brocious, W., Swegle, J., and Cordier, P. 1992. Shock Metamorphism of Quartz with Initial Temperatures –170 to +1000°C. *Physics and Chemistry of Minerals* 19: 267–88. <https://doi.org/10.1007/BF00204005>.
- Grieve, R. A. F., Langenhorst, F., and Stöffler, D. 1996. Shock Metamorphism of Quartz in Nature and Experiment: II. Significance in Geoscience. *Meteoritics & Planetary Science* 31: 6–35. <https://doi.org/10.1111/j.1945-5100.1996.tb02049.x>.
- Hamers, M. F., and Drury, M. R. 2011. Scanning Electron Microscope-Cathodoluminescence (SEM-CL) Imaging of Planar Deformation Features and Tectonic Deformation Lamellae in Quartz. *Meteoritics & Planetary Science* 46: 1814–31. <https://doi.org/10.1111/j.1945-5100.2011.01295.x>.
- Hough, R. M., Lee, M. R., and Bevan, A. W. R. 2003. Characterization and Significance of Shocked Quartz from the Woodleigh Impact Structure, Western Australia. *Meteoritics & Planetary Science* 38: 1341–50. <https://doi.org/10.1111/j.1945-5100.2003.tb00318.x>.
- Howard K. T., Bunopas S., Burrett C. F., Haines P. W., and Norman M. D. 2000. The 770 Ka Tektite Producing Impact Event: Evidence for Distal Environmental Effects in NE Thailand (Abstract #1308). 31st Lunar and Planetary Science Conference. CD-ROM.
- Joreau, P., French, B. M., and Doukhan, J. C. 1996. A TEM Investigation of Shock Metamorphism in Quartz from the Sudbury Impact Structure (Canada). *Earth and Planetary Science Letters* 138: 137–43. [https://doi.org/10.1016/0012-821x\(95\)00236-6](https://doi.org/10.1016/0012-821x(95)00236-6).
- Jourdan, F., Nomade, S., Wingate, M. T. D., Eroglu, E., and Deino, A. 2019. Ultraprecise Age and Formation Temperature of the Australasian Tektites Constrained by $^{40}\text{Ar}/^{39}\text{Ar}$ Analyses. *Meteoritics & Planetary Science* 54: 2573–91. <https://doi.org/10.1111/maps.13305>.
- Keates, S. G. 2000. Tektites and the Age Paradox in Mid-Pleistocene China. *Science* 289: 507. <https://doi.org/10.1126/science.289.5479.507a>.
- Kenkmann, T., Deutsch, A., Thoma, K., Ebert, M., Poelchau, M. H., Buhl, E., Carl, E. R., et al. 2018. Experimental Impact Cratering: A Summary of the Major Results of the MEMIN Research Unit. *Meteoritics & Planetary Science* 53: 1543–68. <https://doi.org/10.1111/maps.13048>.
- Kieffer, S. W. 1971. Metamorphism of the Coconino Sandstone at Meteor Crater, Arizona. *Journal of Geophysical Research* 76: 5449–73. <https://doi.org/10.1029/JB076i023p05449>.
- Koeberl, C. 1992. Geochemistry and Origin of Muong Nong-Type Tektites. *Geochimica et Cosmochimica Acta* 56: 1033–64. [https://doi.org/10.1016/0016-7037\(92\)90046-L](https://doi.org/10.1016/0016-7037(92)90046-L).
- Koeberl, C., and Glass, B. P. 2000. Tektites and the Age Paradox in Mid-Pleistocene China. *Science* 289: 507. <https://doi.org/10.1126/science.289.5479.507a>.
- Kowitz, A., Guldemeister, N., Schmitt, R. T., Reimold, W. U., Wunnemann, K., and Holzwarth, A. 2016. Revision and Recalibration of Existing Shock Classifications for Quartzose Rocks Using Low Shock Pressure (2.5–20 GPa) Recovery Experiments and Mesoscale Numerical Modeling. *Meteoritics & Planetary Science* 51: 1741–61. <https://doi.org/10.1111/maps.12712>.
- Krumbein, W. C. 1941. Measurement and Geological Significance of Shape and Roundness of Sedimentary Particles. *Journal of Sedimentary Petrology* 11: 64–72. <https://doi.org/10.1306/D42690F3-2B26-11D7-8648000102C1865D>.
- Langbroek, M. 2015. Do Tektites Really Date the Bifaces from the Bose (Baise) Basin, Guangxi, Southern China? *Journal of Human Evolution* 80: 175–8. <https://doi.org/10.1016/j.jhevol.2014.06.019>.
- Langenhorst, F. 1994. Shock Experiments on Pre-Heated Alpha-Quartz and Beta-Quartz: II. X-Ray and TEM Investigations. *Earth and Planetary Science Letters* 128: 683–98. [https://doi.org/10.1016/0012-821X\(94\)90179-1](https://doi.org/10.1016/0012-821X(94)90179-1).
- Langenhorst, F. 2002. Shock Metamorphism of Some Minerals: Basic Introduction and Microstructural Observations. *Bulletin of the Czech Geological Survey* 77: 265–82.
- Langenhorst, F., and Deutsch, A. 1996. The Azuara and Rubielos Structures, Spain; Twin Impact Craters or Alpine Thrust Systems? TEM Investigations on Deformed Quartz Disprove Shock Origin (Abstract). 27th Lunar and Planetary Science Conference. pp. 725–26.
- Langenhorst, F., Kyte, F. T., and Retallack, G. J. 2005. Reexamination of Quartz Grains from the Permian-Triassic Boundary Section at Graphite Peak, Antarctica (Abstract #2358). 36th Lunar and Planetary Science Conference. CD-ROM.
- Lee, M. Y., and Wei, K. Y. 2000. Australasian Microtektites in the South China Sea and the West Philippine Sea: Implications for Age, Size, and Location of the Impact Crater. *Meteoritics & Planetary Science* 35: 1151–5. <https://doi.org/10.1111/j.1945-5100.2000.tb01504.x>.
- Leroux, H., and Doukhan, J. C. 1993. Dynamic Deformation of Quartz in the Landslide of Köfels, Austria. *European Journal of Mineralogy* 5: 893–902. <https://doi.org/10.1127/ejm/5/5/0893>.
- Lyons, J. B., Officer, C. B., Borella, P. E., and Lahodinsky, R. 1993. Planar Lamellar Substructures in Quartz. *Earth and Planetary Science Letters* 119: 431–40. [https://doi.org/10.1016/0012-821X\(93\)90151-X](https://doi.org/10.1016/0012-821X(93)90151-X).
- Ma, P., Aggrey, K., Tonzola, C., Schnabel, C., Nicola, P. D., Herzog, G. F., Wasson, J. T., et al. 2004. Beryllium-10 in Australasian Tektites: Constraints on the Location of the Source Crater. *Geochimica et Cosmochimica Acta* 68: 3883–96. <https://doi.org/10.1016/j.gca.2004.03.026>.
- Mansfeld, U., Langenhorst, F., Ebert, M., Kowitz, A., and Schmitt, R. T. 2017. Microscopic Evidence of Stishovite Generated in Low-Pressure Shock Experiments on Porous Sandstone: Constraints on its Genesis. *Meteoritics & Planetary Science* 52: 1449–64. <https://doi.org/10.1111/maps.12867>.

- McGetchin, T. R., Settle, M., and Head, J. W. 1973. Radial Thickness Variation in Impact Crater Ejecta: Implications for Lunar Basin Deposits. *Russian Journal of Mathematical Physics* 20: 226–36. [https://doi.org/10.1016/0012-821X\(73\)90162-3](https://doi.org/10.1016/0012-821X(73)90162-3)
- McLaren, A. C., and Hobbs, B. E. 1972. Transmission Electron Microscope Investigation of Some Naturally Deformed Quartzites. In *Flow and Fracture of Rocks*, edited by H. C. Heard, I. Y. Borg, N. L. Carter, and C. B. Raleigh, 55–66. Washington, D.C.: American Geophysical Union.
- Minezaki, T., Hisada, K., Hara, H., and Kamata, Y. 2019. Tectono-Stratigraphy of Late Carboniferous to Triassic Successions of the Khorat Plateau Basin, Indochina Block, Northeastern Thailand: Initiation of the Indosinian Orogeny by Collision of the Indochina and South China Blocks. *Journal of Asian Earth Sciences* 170: 208–24. <https://doi.org/10.1016/j.jseaes.2018.10.020>.
- Nakano, Y., Goto, K., Matsui, T., Tada, R., and Tajika, E. 2008. PDF Orientations in Shocked Quartz Grains Around the Chicxulub Crater. *Meteoritics & Planetary Science* 43: 745–60. <https://doi.org/10.1111/j.1945-5100.2008.tb00682.x>.
- Nuchanong, T., Chaodumrong, P., Luengingkasoot, M., Burrett, C., Techawan, S., Silakul, T., Stokes, R. B., et al. 2014. *Geology of Thailand*. Bangkok: Bureau of Geological Survey, Department of Mineral Resources. 507.
- Ocampo, A. C., Pope, K. O., and Fischer, A. G. 1996. Ejecta Blanket Deposits of the Chicxulub Crater from Albion Island, Belize. *Geological Society of America Special Paper* 307: 75–88. <https://doi.org/10.1130/0-8137-2307-8.75>.
- Pierazzo, E., and Artemieva, N. 2012. Local and Global Environmental Effects of Impacts on Earth. *Elements* 8: 55–60. <https://doi.org/10.2113/gselements.8.1.55>.
- Pope, K. O., Ocampo, A. C., Fischer, A. G., Alvarez, W., Fouke, B. W., Webster, C. L., Vega, F. J., Smit, J., Fritsche, A. E., and Claeys, P. 1999. Chicxulub Impact Ejecta from Albion Island, Belize. *Earth and Planetary Science Letters* 170: 351–64. [https://doi.org/10.1016/S0012-821X\(99\)00123-5](https://doi.org/10.1016/S0012-821X(99)00123-5).
- Prasad, M. S., Mahale, V. P., and Kodagali, V. N. 2007. New Sites of Australasian Microtektites in the Central Indian Ocean: Implications for the Location and Size of Source Crater. *Journal of Geophysical Research* 112: E06007. <https://doi.org/10.1029/2006JE002857>.
- Quintana, S. N., Schultz, P. H., and Horowitz, S. S. 2018. Experimental Constraints on Impact-Induced Winds. *Icarus* 305: 91–104. <https://doi.org/10.1016/j.icarus.2017.12.042>.
- Racey, A., Love, M. A., Canham, A. C., Goodall, J. G. S., Polachan, S., and Jones, P. D. 1996. Stratigraphy and Reservoir Potential of the Mesozoic Khorat Group, NE Thailand Part 1: Stratigraphy and Sedimentary Evolution. *Journal of Petroleum Geology* 19: 5–40. <https://doi.org/10.1111/j.1747-5457.1996.tb00511.x>.
- Reimold, W. U., Crósta, A. P., Hasch, M., Kowitz, A., Hauser, N., Sanchez, J. P., Simões, L. S. A., de Oliveira, G. J., and Zaag, P. T. 2019. Shock Deformation Confirms the Impact Origin for the Cerro Do Jarau, Rio Grande Do Sul, Brazil, Structure. *Meteoritics & Planetary Science* 54: 2384–97. <https://doi.org/10.1111/maps.13233>.
- Reimold, W. U., Ferrière, L., Deutsch, A., and Koeberl, C. 2014. Impact Controversies: Impact Recognition Criteria and Related Issues. *Meteoritics & Planetary Science* 49: 723–31. <https://doi.org/10.1111/maps.12284>.
- Retallack, G. J., Seyedolali, A., Krull, E. S., Holser, W. T., Ambers, C. P., and Kyte, F. T. 1998. Search for Evidence of Impact at the Permian-Triassic Boundary in Antarctica and Australia. *Geology* 26: 979–82. [https://doi.org/10.1130/0091-7613\(1998\)026<0979:SFEIOA>2.3.CO;2](https://doi.org/10.1130/0091-7613(1998)026<0979:SFEIOA>2.3.CO;2).
- Schmieder, M., and Kring, D. A. 2020. Earth's Impact Events Through Geologic Time: A List of Recommended Ages for Terrestrial Impact Structures and Deposits. *Astrobiology* 20: 91–141. <https://doi.org/10.1089/ast.2019.2085>.
- Schneider, C. A., Rasband, W. S., and Eliceiri, K. W. 2012. NIH Image to ImageJ: 25 Years of Image Analysis. *Nature Methods* 9: 671–5. <https://doi.org/10.1038/nmeth.2089>.
- Schnetzler, C. C. 1992. Mechanism of Muong Nong-Type Tektite Formation and Speculation on the Source of Australasian Tektites. *Meteoritics* 165: 154–65. <https://doi.org/10.1111/j.1945-5100.1992.tb00743.x>.
- Schnetzler, C. C., and McHone, J. F. 1996. Source of Australasian Tektites: Investigating Possible Impact Sites in Laos. *Meteoritics & Planetary Science* 31: 73–6. <https://doi.org/10.1111/j.1945-5100.1996.tb02055.x>.
- Schulte, P., Alegret, L., Arenillas, I., Arz, J. A., Barton, P. J., Bown, P. R., Bralower, T. J., et al. 2010. The Chicxulub Asteroid Impact and Mass Extinction at the Cretaceous-Paleogene Boundary. *Science* 327: 1214–8. <https://doi.org/10.1126/science.1177265>.
- Schultz, P. H. 1992. Atmospheric Effects on Ejecta Emplacement and Crater Formation on Venus from Magellan. *Journal of Geophysical Research: Planets* 97: 16183–248.
- Schultz, P. H., and Quintana, S. N. 2017. Impact-Generated Winds on Mars. *Icarus* 292: 86–101. <https://doi.org/10.1016/j.icarus.2017.03.029>.
- Schwarz, W. H., Trieloff, M., Bollinger, K., Gantert, N., Fernandes, V. A., Meyer, H. P., Povenmire, H., Jessberger, E. K., Guglielmino, M., and Koeberl, C. 2016. Coeval Ages of Australasian, Central American and Western Canadian Tektites Reveal Multiple Impacts 790 Ka Ago. *Geochimica et Cosmochimica Acta* 178: 307–19. <https://doi.org/10.1016/j.gca.2015.12.037>.
- Sieh, K., Herrin, J., Jicha, B., Angel, D. S., Moore, J. D. P., Banerjee, P., Wiwegwin, W., et al. 2020. Australasian Impact Crater Buried Under the Bolaven Volcanic Field, Southern Laos. *Proceedings of the National Academy of Sciences of the United States of America* 117: 1346–53. <https://doi.org/10.1073/pnas.1904368116>.
- Songtham, W., Duangkayom, J., and Jintasakul, P. 2012. An Australasian Tektite from the Yasothon Soil Series, Noen Sa-Nga, Chaiyaphum, Northeastern Thailand. *Acta Geoscientia Sinica* 33: 59–64. <https://doi.org/10.3975/cagsb.2012.s1.28>.
- Songtham, W., Mildenhall, D. C., Jintasakul, P., and Duangkayom, J. 2011. Evidence of Sedimentary Deposits Generated by an Early Pleistocene Meteor Impact in Northeastern Thailand. *Proceedings, International Conference on Geology, Geotechnology and Mineral Resources of Indochina (GEOINDO 2011)*, 66–71.
- Stöffler, D., Hamann, C., and Metzler, K. 2018. Shock Metamorphism of Planetary Silicate Rocks and Sediments: Proposal for an Updated Classification System. *Meteoritics & Planetary Science* 53: 5–49. <https://doi.org/10.1111/maps.12912>.

- Stöffler, D., and Langenhorst, F. 1994. Shock Metamorphism of Quartz in Nature and Experiment: I. Basic Observation and Theory. *Meteoritics* 29: 155–81. <https://doi.org/10.1111/j.1945-5100.1994.tb00670.x>.
- Tada, T., Tada, R., Chansom, P., Songtham, W., Carling, P. A., and Tajika, E. 2020. In Situ Occurrence of Muong Nong-Type Australasian Tektite Fragments from the Quaternary Deposits Near Huai Om, Northeastern Thailand. *Progress in Earth and Planetary Science* 7: 66. <https://doi.org/10.1186/s40645-020-00378-4>.
- Takashimizu, Y., and Iiyoshi, M. 2016. New Parameter of Roundness R: Circularity Corrected by Aspect Ratio. *Progress in Earth and Planetary Science* 3: 2. <https://doi.org/10.1186/s40645-015-0078-x>.
- Tamura, T. 1992. Landform Development and Related Environmental Changes in the Chi River Basin, Northeast Thailand. In *The Science Reports of the Tohoku University*, 7th series (geography) ed., vol. 42, 107–27. Sendai: Faculty of Science, Tohoku University.
- Teraoka, Y., and Okumura, K. 2011. *The Geological Map of Asia (at 1:5,000,000 Scale)*. Tsukuba: Geological Survey of Japan, AIST.
- Van Hoesel, A., Hoek, W. Z., Pennock, G. M., Kaiser, K., Plümper, O., Jankowski, M., Hamers, M. F., et al. 2015. A Search for Shocked Quartz Grains in the Allerød-Younger Dryas Boundary Layer. *Meteoritics & Planetary Science* 50: 483–98. <https://doi.org/10.1111/maps.12435>.
- Vernooij, M. G. C., and Langenhorst, F. 2005. Experimental Reproduction of Tectonic Deformation Lamellae in Quartz and Comparison to Shock-Induced Planar Deformation Features. *Meteoritics & Planetary Science* 40: 1353–61. <https://doi.org/10.1111/j.1945-5100.2005.tb00406.x>.
- von Engelhardt, W., and Bertsch, W. 1969. Shock Induced Planar Deformation Structures in Quartz from the Ries Crater, Germany. *Contributions to Mineralogy and Petrology* 20: 203–34. <https://doi.org/10.1007/BF00377477>.
- Wasson, J. T., Pitakpaivan, K., Putthapiban, P., Salyapongse, S., Thaothimthong, B., and McHone, J. F. 1995. Field Recovery of Layered Tektites in Northeast Thailand. *Journal of Geophysical Research* 100: 14383–9. <https://doi.org/10.1029/95JE01504>.
- White, S. 1973. Deformation Lamellae in Naturally Deformed Quartz. *Nature Physical Science* 245: 26–8. <https://doi.org/10.1038/physci245026a0>.
- Wongsomsak, S. 1986. Salinization in Northeast Thailand. *Southeast Asian Studies* 24: 133–53.
- Yamei, H., Potts, R., Baoyin, Y., Zhengtang, G., Deino, A., Wei, W., Clark, J., Guangmao, X., and Weiwen, H. 2000. Mid-Pleistocene Acheulan-Like Stone Technology of the Bose Basin, South China. *Science* 287:1622–6. <https://www.science.org/doi/10.1126/science.287.5458.1622>

SUPPORTING INFORMATION

Additional supporting information may be found in the online version of this article.

Appendix S1.

Appendix S2.